

**NANOMATERIAL PROCESSING FOR MULTIFUNCTIONAL
PATTERNED COMPOSITES FOR *IN SITU* SENSING APPLICATIONS**

by

Zachary R. Melrose

A thesis submitted to the Faculty of the University of Delaware in partial fulfillment
of the requirements for the degree of Master of Science in Mechanical Engineering

Summer 2014

© 2014 Melrose
All Rights Reserved

UMI Number: 1567816

All rights reserved

INFORMATION TO ALL USERS

The quality of this reproduction is dependent upon the quality of the copy submitted.

In the unlikely event that the author did not send a complete manuscript and there are missing pages, these will be noted. Also, if material had to be removed, a note will indicate the deletion.



UMI 1567816

Published by ProQuest LLC (2014). Copyright in the Dissertation held by the Author.

Microform Edition © ProQuest LLC.

All rights reserved. This work is protected against unauthorized copying under Title 17, United States Code



ProQuest LLC.
789 East Eisenhower Parkway
P.O. Box 1346
Ann Arbor, MI 48106 - 1346

**NANOMATERIAL PROCESSING FOR MULTIFUNCTIONAL
PATTERNED COMPOSITES FOR *IN SITU* SENSING APPLICATIONS**

by

Zachary R. Melrose

Approved: _____
Dr. Erik T. Thostenson, Ph.D.
Professor in charge of thesis on behalf of the Advisory Committee

Approved: _____
Dr. Suresh G. Advani, Ph.D.
Chair of the Department of Mechanical Engineering

Approved: _____
Dr. Babatunde. A. Ogunnaike, Ph.D.
Dean of the College of Engineering

Approved: _____
James G. Richards, Ph.D.
Vice Provost for Graduate and Professional Education

ACKNOWLEDGMENTS

I'd like to express my gratitude to Professor Thostenson for his assistance and guidance throughout my graduate studies. He has mentored me since my undergraduate work, and I've learned much about research through his efforts.

To my loving family, Jeff, Karen, Gillian, and Hepburn, thank you for supporting me throughout my educational endeavors and always being there for me

I'd like to recognize the Department of Defense (DoD) which has supported me through the National Defense Science & Engineering (NDSEG) Graduate Fellowship Program and I thank them for their continued support.

This research was sponsored by the Army Research Laboratory and was accomplished under Cooperative Agreement Number W911NF-07-2-0026. The views and conclusions contained in this document are those of the author and should not be interpreted as representing the official policies, either expressed or implied, of the Army Research Laboratory or the U.S. Government.

"I have a realistic grasp of my own strengths and weaknesses. My mind is my weapon. My brother has his sword, King Robert has his warhammer, and I have my mind... and a mind needs books as a sword needs a whetstone, if it is to keep its edge. That's why I read so much, Jon Snow."

Tyrion Lannister, *A Song of Fire and Ice*
George R.R. Martin

TABLE OF CONTENTS

LIST OF TABLES	vii
LIST OF FIGURES	viii
ABSTRACT	xii
Chapter	
1 INTRODUCTION AND BACKGROUND	1
1.1 Introduction	1
1.2 Structural Health Monitoring and Non-Destructive Evaluation.....	2
1.3 Statistical Nature of Composite Failure	3
1.4 In Situ Approach to Damage Sensing	5
1.5 Graphene Nanocomposites	6
1.6 Scalable Nanocomposite Processing	9
1.7 Research Statement	10
2 MATERIALS AND METHODS	12
2.1 Electrical Conductivity through Nano-Material Dispersion.....	12
2.1.1 xGnP Nanocomposite	12
2.1.2 Patterned Hybrid Nanocomposite.....	14
2.1.2.1 Patterning Media Synthesis	14
2.1.2.2 Patterning Media and Nanomaterial Integration	15
2.2 Composite Manufacture and Electrical Testing Preparation.....	16
2.2.1 xGnP Nanocomposite Tensile Bar	16
2.2.2 Patterned Sensor Composite	17
2.2.2.1 Adapted Screen Printing Process.....	17
2.2.2.2 Composite Preparation	18
2.3 Coupled Mechanical, Electrical, and Acoustic Characterization	19
2.4 Summary.....	20
3 xGnP NANOCOMPOSITE PROCESSING FOR SELF-SENSING APPLICATIONS.....	21
3.1 Introduction	21
3.2 Assessment of Multifunctional Performance	21
3.3 Damage Onset and Propagation	30

3.4	Real-Time Damage Response	36
3.5	Summary.....	37
4	HIERARCHICAL PATTERNING FOR <i>IN SITU</i> INTERFACIAL SENSING	38
4.1	Introduction	38
4.2	Quasi-Static Tensile Tests	38
4.3	Transient Damage Sensing Response.....	45
4.4	Time-Invariant NDE Approaches.....	48
4.5	Analysis of Damage Progression and Failure Mechanisms for SHM.....	50
4.6	Summary.....	57
5	CONCLUSIONS AND FUTURE WORK.....	59
5.1	Conclusions	59
5.2	Future Work.....	60
5.2.1	Processing and Characterization Methods.....	60
5.2.1.1	xGnP Microscopy Study.....	60
5.2.1.2	Inkjet Printing	61
5.2.1.3	Functionalized and Reformulated Inks.....	62
5.2.2	Experimental Studies.....	63
5.2.2.1	Sensing of Failure in Single Fiber Lamina.....	63
5.2.2.2	Cross-Ply Composite Studies	63
	REFERENCES	65
Appendix		
A	DATA ACQUISITION SYSTEM	70
A.1	Introduction	70
A.1.1	Hardware	72
A.1.1.1	Equipment list.....	72
A.1.2	Pictorial guide for equipment use.....	72
A.2	Troubleshooting.....	76

A.2.1	Measurement and Automation Explorer (MAX)	76
A.2.2	DMM Soft Front Panel	76
A.2.3	NI Switch Soft Front Panel.....	76
A.2.4	NI LabVIEW SignalExpress	77
A.3	Software.....	77
A.3.1	Programs and Usage	77
B	CITATION NOTE.....	80
B.1	Figure and Table Originality	80

LIST OF TABLES

Table 2.1:	Processing parameters for patterning media	16
Table 4.1:	Carbon nanotube & xGnP mechanical and electrical properties ..	44

LIST OF FIGURES

Figure 1.1: Illustration of carbon nanotubes selectively modified bonded joint for damage sensing [23].	6
Figure 2.1: Electron micrographs showing xGnP (a), and carbon nanotubes (b), in their as-received state. The difference in nanomaterial feature size is apparent in the difference scales for each micrograph.	13
Figure 2.2: Illustration of nanocomposite tensile bar.	17
Figure 2.3: Illustration of a tensile bar with a patterned sensor.	19
Figure 3.1: Processing intensity effects on xGnP: (a) resistivity and (b) strength at the different processing intervals.	22
Figure 3.2: Electron micrographs of a fracture surface. (a) Material processed at a 100 μm gap showing the platelets well dispersed throughout the matrix. Thermodynamic instability due to the xGnP particle dispersion in a polar matrix material leads to the re-agglomeration of xGnP into clusters. (b) Clusters shown in materials processed at a 60 μm gap setting are found throughout the nanocomposite and form the electrically conductive network.	24
Figure 3.3: Electron micrographs of a fracture surfaces of the xGnP nanocomposites. (a) Nanocomposites processed at a 80 μm gap shows numerous large platelets. The thermodynamic instability produces only a few clusters, reducing the overall electrical conductivity. (b) Material processed at gap settings of 40 μm showing a highly textured fracture surface, with smaller platelets sparsely distributed. Few xGnP particles remain intact, explaining the low conductivity of the nanomaterial.	25
Figure 3.4: Electron micrograph showing xGnP oriented perpendicular to the fracture surface, indicating that the platelets act as defects where the crack propagated. xGnP aligned parallel to the fracture surface is not visible. Their adhesion between the exterior basal planes and matrix exceeds the strength of perpendicular aligned plates, whose strength is dominated by inter-planar shear strength.	26
Figure 3.5: (a) Piezoresistivity illustration of effects on carbon nanotube dispersion conductive pathways subjected to compressive, zero, and tensile strains and the associated (b) resistance-strain response.	27

Figure 3.6:	(a) Typical stress, normalized resistance- strain loading curve of 60 μm . (b) Processing intensity effects on gage factor.	29
Figure 3.7:	Transient resistance change and AE cumulative counts during progressive cyclic loading with materials processed at (a) 100 μm , and (b) 60 μm	31
Figure 3.8:	Damage-sustaining cycle illustrated to define relevant terms and parameters of the resistance signal. Elastic response and crack reopening are associated with the first part of the resistance response. Beyond the knee in the resistance response, new damage is incurred where the xGnP layers separate. During unloading the cracks that opened during loading close.	32
Figure 3.9:	Stress-strain plot showing stiffness loss after the second cycle.	33
Figure 3.10:	(a) Regional assignment for crack reopening (CR), new damage (ND), and crack closure (CC), and (b) curv fits from each region during load cycles, increasing by 444.82N per cycle.	34
Figure 4.1:	Characteristic responses of patterned (a) carbon nanotube and (b) xGnP sensors.	40
Figure 4.2:	Optical micrograph of carbon nanotube (a) onto glass fibers showing the coverage and distribution of material and illustration (b).	42
Figure 4.3:	Optical micrograph of xGnP (a) on glass fibers showing the coverage and distribution of material and illustration (b).	43
Figure 4.4:	(a) Cyclic loading-displacement-resistance plots for carbon nanotube sensor and (b) resistance-strain plot.	46
Figure 4.5:	(a) Cyclic loading-displacement-resistance plots for xGnP sensor and (b) resistance-strain plot.	47
Figure 4.6:	Baseline method for carbon nanotube (a) and xGnP (b) sensing networks subjected to progressive cyclic tensile loading.	49
Figure 4.7:	(a) Carbon nanotube cyclic response with AE emissions, and a illustrate depicting the macro-, micro-, nano-scale structure of (b) idealized and (c) real world composites.	52

Figure 4.8:	(a) Plot of the 3 rd , 4 th , 5 th cycle, where damage first initiates, as indicated by the circled AE events. The dashed green lines indicate a change in the mechanism affecting the resistance response. The illustrations highlight the differences in the state of stress in composites with initial fiber fractures under no applied load (b) and with applied load (c).....	54
Figure 4.9:	(a) Plot of 7 th , 8 th , and 9 th load cycle during the transition to a new damage mechanism, where (b) illustrates the state of stress prior to the shift, and (c) the complex state of stress afterwards.....	56
Figure 4.10:	Optical micrograph of protruding fibers indicative of fiber debonding from the matrix at the carbon nanotube fracture surface within the patterned region.	57
Figure 5.1:	Screen printing versus inkjet printing.	62
Figure A.1:	Picture of data acquisition system built into a cart.....	71
Figure A.2:	The analog signal card is located in the fourth slot of the chassis, and has eight channels labeled 0 to 7 that can be interfaced. Channels zero to three are wired to the bulkhead in Figure A.5).	72
Figure A.3:	The eight channel strain bridge terminal block is wired for quarter-bridge configurations, but half- and full- strain bridge configurations are possible.	73
Figure A.4:	The multiplexer terminal block sits in the eighth slot of the chassis and has four regions of which three have been interfaced with the ribbon cable. Two ribbon cables are required to use each of the four regions. These regions have two sets of 16 nodes, labeled 0 to 15 and 16 to 32. Additional ribbon cable and terminal blocks are stored on the cart for swapping out cable for new multiplexing applications, i.e. reconfiguring a two wire to four-wire multiplexer. Current configuration on the first two regions is for two wire multiplexing across 30 distinct regions and is instrumented in the upper half of the wiring data panel in Figure A.5.....	74
Figure A.5:	The wiring panel built in the cart serves as a wire pass through or bulkhead. Additionally the reconfigurable nature of the components allows for the simple redesign for new experiments. A 30 channel, two wire multiplexer in positioned in the upper half of the panel. The lower half has four BNC pass through slots for the strain bridge (S3-#) and four analog signals (S4-#).....	75

Figure A.6: Front panel of data acquisition system configured to monitor six different resistance signals. Constants from instron are entered first for crosshead extension and for the load cell. Extension and load indicators are positioned along the Y axis of the stacked plots for direct comparison to load frame values. Specimen dimensions are inputted to calculate stress. Data is gathered into two files that the user can specify the location of, one for resistance and the second for stress and strain. This version configuration is designed to multiplex resistance measurements across six nodes, and display the response in the right hand side plot. 78

Figure A.7: Object based coding used to construct the .vi file. Users should use [control] and [h] to learn the purpose of any coding element that is not understood. The load icon controls the functions of strain and analog signals in cards three and four. The DMM icon controls the multi-meter function and switching capabilities of cards seven and eight. 79

ABSTRACT

The increasing performance demands on composite materials have stimulated the development of new approaches and manufacturing techniques to integrate various system functionalities within the composite structure. Opportunity exists to produce smart, self-sensing composites, by altering the microstructure of the composite where sensors can be patterned for assessing damage locality and severity. Introduction of nanomaterials into continuous fiber-reinforced composites either at the fiber/matrix interface or within the polymer matrix enables further tailoring of mechanical and electrical properties. Carbon nanotubes have been studied extensively for modifying the mechanical and physical properties of fiber composites. Recently graphene has generated scientific and technical interest due to potential lower raw material costs and ease of processing.

This work studies graphene nano-platelet processing parameters to determine the suitability of graphene nanocomposites for *in situ* sensing applications. Processing parameters for optimizing the piezoresistive response of graphene nano-platelet composites for *in situ* sensing applications are determined and applied in for the development of a patterning media suitable for deposition onto glass fibers.

A new approach to selectively modify the electrical properties of composite fibers is employed to selectively deposit carbon nanotube and graphene nano-platelet enhanced patterning media through an adapted screen printing process. These nano-modified depositions create hierarchical patterns of piezoresistive sensors as fully integrated components and form a distributed sensor network at the fiber/matrix interface.

New analysis tools for resistance based sensing techniques are applied to nanocomposites and patterned unidirectional hybrid nanocomposites to assess damage onset and accumulation. The sensitivity of the electrical response for the graphene nano-platelet is compared with the electrical response of the carbon nanotube networks. Real-time monitoring of the electrical resistance change is then utilized to shed light on the nature and progression of damage in the composite.

Chapter 1

INTRODUCTION AND BACKGROUND

1.1 Introduction

Composite materials are currently used in the aviation, naval, automotive, and sporting & recreational industries for high performance applications. The high stiffness and strength of composites is complimented by the material's low density and allows for use in weight-sensitive applications. These desirable engineering properties are a consequence of the synergistic interaction of the reinforcing fibers with the matrix.

The ability to design specific properties into a final composite through the selection of the constituent materials and controlling the composite microstructure is often a composite's greatest strength and weakness. Inhomogeneity in the material composition results in complicated failure mechanisms that can result in catastrophic material failure. Micro-scale damage reduces durability and service life of materials and is difficult to detect. Material validation and re-certification is often required and the high associated cost can limit future composite integration into structures.

Nano-scaled materials can be added to composites to improve material properties or add additional functionalities. This offers an engineer a further degree of control for designing composites. Damage sensing with carbon nanotubes has proven effective for sensing micro-scale damage within composites but it is still an emerging method requiring further research. Graphene has displayed a wide range of unique properties and is being studied for potential future applications.

In this research two primary questions were addressed: (1) “Can we make a graphene in situ damage sensor?” and (2) “How can we sense damage in specific areas of a composite?”

1.2 Structural Health Monitoring and Non-Destructive Evaluation

Recent advances in the manufacture of fiber-reinforced composite have not been fully realized due to the limited progress on economical component validation and re-certification of structural components. Many vehicles could benefit from the weight savings associated with upgrading components to the lighter weight composite alternatives. Structures intended for human use are subject to more rigorous standards which generally increase the operating and maintenance costs. To achieve a small share of the potential weight savings, manufacturers have largely relegated the use of composites to non-structural components which are subject to less stringent standards.

Recent efforts to incorporate composites into critical structural applications have renewed interest in developing non-destructive evaluation (NDE) methods to satisfy safety standards at a lower cost. The intermittent servicing and NDE testing schedules are effective for monitoring fatigue damage but are not well suited to address sudden damage that can precipitate a catastrophic failure of the composite.

Active, real-time sensors are utilized in the structural health monitoring (SHM) approach, where densely populated grids of individual sensors are networked into a system level-solution. The damage sensing resolution of a SHM system is directly related to the extent of sensor implementation, creating a tradeoff in having a robust sensing network versus the performance loss associated with the multitude of obtrusive sensors affixed and cabled throughout the structure. A way to achieve the desired functionality of a low weight, self-sensing structure would be to deploy a

selectively integrated sensor network hierarchically positioned in high risk, or ‘hot spot’ locations. Recent studies into integrated sensors explore fiber optic cables [1, 2], imbedded piezoelectric transducers [3, 4, 5], strain [6], shape memory alloys [7], time domain reflectometry [8], and nanomaterial [9, 10] based options. These sensing technologies are well suited to indirectly assess the extent of damage, but they have limited ability to recognize and distinguish individual micro-scale damage mechanisms that cumulate in the ultimate failure of a composite.

1.3 Statistical Nature of Composite Failure

Understanding the nature and progression of damage in unidirectional composites is statistical in nature, owing to the wide distribution in fiber strengths, discussed by Weibull [11]. The fracture of a brittle fiber is defect-driven, which can be modeled as a chain consisting of links of different strengths. This is referred to as the weakest link theory. In a composite the failure of any one link along a fiber results in a local stress concentration at the fiber fracture point. Stress is redirected through the surrounding matrix via shear to nearby load-carrying fibers and was modeled by Rosen [12]. Rosen and Zweben [13] presented a statistical model for local stress magnification which results in a propagation of fiber breakage in the immediate vicinity of the initial failure of its nearest neighboring fiber [14]. A similar phenomenon occurs within the lamina at the fiber bundle level and precipitates the ultimate failure of the composite structure. Means to directly measure the fracture of fibers within a composite was first demonstrated by Schulte [15, 16] who used direct current measurements of carbon fiber composites to monitor resistance changes resulting from fiber and bundle failures during loading.

Additional considerations must be taken for the matrix material strength and adhesion to the fibers as it directly relates to the material's ability to transmit shear between fibers and is studied through shear lag analysis. Sensing throughout the bulk matrix by monitoring the resistance change of dispersed carbon nanotubes was first demonstrated by Thostenson *et al.* [17], which proved sensitive to transverse crack propagation in cross-ply composites as well as interlaminar cracks and delamination. The fiber/matrix interphase region is prone to failure due to the poor adhesion and the local difference in material stiffness. Consequently, specific damage mechanisms and sensing challenges exist in this region.

Assuming the interphase between the fiber and matrix still transmits shear after failure of the weak fibers, elastic deformation, plastic flow, and cracking of the polymer matrix can occur depending upon the strength and proximity to intact fibers. Crack propagation from fiber fracture can be blunted by nearby fibers that fail adhesively at the surfaces due to the stress concentration of the crack [18]. Adhesive failure the fiber interface will result in fiber debonding followed by frictional sliding [19].

The complicated nature of the composite fracture mechanism resulting from the material's properties in the longitudinal, transverse, and through-thickness directions require additional consideration. Long-term durability concerns focus on matrix-dominated failures where cracks between fibers in matrix rich regions and delamination between plies precipitate failure [20]. In-plane failure results from fracture of the load carrying fibers but is preempted by matrix cracking around failed fiber ends. Sensing cracks within the matrix in both matrix-rich regions and fiber/matrix interface is challenging, but it would serve as a reliable indicator of

composite health. This difficulty in assessing the structural integrity of composites can limit their applications and often results in over-design of composite materials. In addition, the structural variability towards traditional alternatives, i.e. metals, if the uncertainty in composite durability persists.

Various modes of damage in unidirectional composites have been discussed here to highlight the need for sensing tools directed at the interphase region; however to the author's knowledge no direct methods exist to monitor these phenomena in bulk composites.

1.4 In Situ Approach to Damage Sensing

Current structural assessment methods focus on sensing at discrete points or regions through observation of macro-scale phenomena that results from an accumulation of micro-scale fracture events. Introduction of nanoscale materials into composite system for the development of hierarchically modified advanced multifunctional composites has generated significant interest within academia, and has been recently reviewed by Bismarck [21].

Sensors based on nanomaterials are uniquely capable to provide insight on the state of micro-scale damage in addition to macro scale damage [22]. Thostenson [10] first demonstrated the processing-structure multifunctional relationship in carbon nanotubes and epoxy composites for the sensing of damage in the matrix where the extension of the specimen's *in situ* electrically conductive nano-network drives a stochastic process that separates and severs the percolating electrical pathways, degrading the network's electrical conductivity or increasing its resistivity. Electrical conductivity is an intrinsic material property which allows intermittent, as opposed to

continuous, sensing to assess the extent of damage. Values are compared with a baseline value in either real-time for SHM or intermittently within a NDE system.

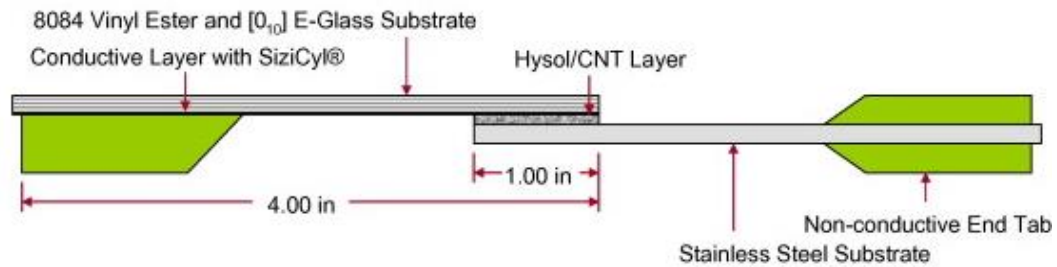


Figure 1.1: Illustration of carbon nanotubes selectively modified bonded joint for damage sensing [23].

Prior research efforts have produced piezoresistive sensors either through the nanomaterial dispersed in a matrix material [24] or nanoscale deposition on reinforcing fibers, as demonstrated by Lim and co-workers [23], where a self-sensing adhesively bonded hybrid steel / composite joint has a carbon nanotubes selectively modified fiber ply for damage monitoring along the bond interface. These modifications yield a nanomaterial-enhanced structure suitable for linear scans across the adhesive joint.

1.5 Graphene Nanocomposites

Graphene presents an alternative nanomaterial for the *in situ* sensing approach given its similar high electrical conductivity and strength to carbon nanotubes, and presents new opportunities owing to its distinct morphology. Recent advances in graphite exfoliation for graphene production and commercialization have dramatically reduced the cost of the material, enabling a wide range of research on practical

applications. Graphene nano-platelets (xGnP) have seen use in a wide range of applications to harness the materials mechanical [7, 25-27], electrical [27], thermal [28], chemical & biological [29, 30], and optical [31, 32] properties. Graphene is an interesting alternative nanomaterial for *in situ* sensing due to its planar geometry which requires exfoliation of the individual graphene sheets. In contrast, bulk carbon nanotubes are generally produced in an entangled agglomerated form and are dispersed with mechanically methods or through chemical methods that reduce nanotube length.

The challenge of bridging the nano-to-macro scale divide is a difficult one, as creating macro scale pieces of pristine graphene is not yet economically feasible. Another option of using smaller, imperfect pieces of graphene in conjunction with a supportive matrix to form a nanocomposite is explored here. Current research efforts focus on the development of polymers reinforced with a graphene-like material to exploit the material's nanoscale properties to enhance electrical and mechanical performance [33] or to add additional application-specific functionalities. Many different nanomaterials comprised of planar sheets of hexagonally bonded carbon atoms have been studied and are typically identified as graphene, a few layers of graphene, and graphite flakes. The processes of obtaining a 2-D, single atom thick material is a scientific and technical challenge. The dispersion techniques are generally classified as chemical and mechanical exfoliation approaches.

Chemical graphene dispersion methods focus on either edge or planar functionalization. Bonding to the edge of graphene platelets is easier due to the higher rate of defective sites in the carbon lattice, serving as points of attachment; however modification of the circumferential area of the edges has limited ability to achieve a

stable dispersion [34]. Additional sites for chemical bonding along the planar surface by implanting or utilizing existing defects are produced at the expense of the mechanical and electrical properties [34].

The chemical reduction of graphite produces stable dispersions using hydrazine, a highly toxic and unstable material [35]. Various methods, including some environmentally friendly 'Green' methods can produce graphene oxide, a water-soluble material that has high stiffness and strength but low electrical conductivity [36]. Graphene oxide is graphene sheets chemically bonded with hydroxyl groups at defective sites in the carbon lattice. Researchers believe this material could serve as an intermediary to produce graphene.

Mechanical exfoliation methods utilize shear forces to separate layers, the most famous being the 'scotch tape method', where layers are sheared from a piece graphite one at a time [37]. Other methods utilize aqueous dispersions where high power ultrasonic probes create hydrodynamic inertial cavitations of microscopic bubbles which rapidly collapse creating shear forces [38]. The aqueous nature lends itself to either water soluble polymers or solvent exchange methods for polymer introduction. These solvent-based dispersions are suited for thermoplastics and are used for solution casting or filtration methods to produce nanocomposite films or composites of limited sizes. Injection molding can be employed, where the high viscosity of the polymer melt being agitated by a screw extruder exfoliates the graphite during extrusion.

Calendering mills, as employed in this work, shear graphite flakes with counter rotating drums, and is used for processing viscous liquids and intercalated materials. Manufacturing of nanocomposites has focused primarily on thermoplastics like polystyrene (PS), polyvinyl- alcohol (PVA), thermoplastic polyurethane (TPU),

polyethylene (PE), and polycarbonate (PC) over thermosetting resin such as epoxies and vinyl esters.

Nanocomposite manufacture requires special attention to the reactive properties of the high surface area material. Chemical interactions with solvents or intermediary materials during manufacture can chemically modify the material, changing its properties. The dispersion process can result in the degradation of nanoscale additive and negate any synergistic gain from its incorporation.

1.6 Scalable Nanocomposite Processing

Full integration of nanocomposite sensors into a large structure is currently impractical due to high material and processing costs. Nanomaterials hierarchically patterned across a structure create sensing regions at points of interest which enables scalable health monitoring systems. Industrially-viable processes to deposit the nano-enhanced media in the predetermined positions present an additional opportunity to reduce production costs when employed over the existing approaches of modifying the entire structure with nanomaterials.

Screen printing is a mature, commercialized technology that utilizes a non-permeable stencil supported by a porous mesh. Ink transfers through the exposed mesh and prints onto the desired substrate. When adapted to composite processing with an aqueous suspension of nanomaterials, deposition onto composite fibers in a controlled, consistent manner is possible and can be used for creating hierarchically scaled composites. Upon solvent removal, individual laminae can be placed into a fiber preform for composites manufacturing via resin transfer molding. The distribution of patterned sensors throughout a composite can create a multi-scale damage sensing network for gathering information on structural health.

Composites manufacturing with this adapted screen printing technique is amenable for scale-up and requires minimal modification of conventional processing techniques. Currently woven fiber mats arrive on rolls and are positioned so that the material feeds directly into an automated fiber cutting machine or station. After cutting, material is positioned into a mold then prepared for resin transfer molding. An intermediary step prior to cutting consisting of a screen printer and flash dryer before the fiber cutting station would maintain the roll-to-roll flow of material in a commercial composite manufacturing environment.

1.7 Research Statement

This work expands upon carbon nanotube damage sensing and establishes a fundamental understanding of *in situ* sensing with graphene and enables the exploration of multifunctional applications. Graphene nano-platelet (xGnP, XG Sciences, Inc.) nanocomposites are mechanically dispersed under different shear intensities to determine appropriate processing conditions for dispersion in a thermosetting matrix with the desired piezoresistive electrical/mechanical response. Nanocomposite tensile bars are processed at varied conditions for evaluation under quasi static monotonic and cyclic loading conditions for analysis of the damage onset and accumulation behavior.

The *in situ* sensing approach from globally modified composites to hierarchal patterned glass fiber reinforced composites suitable for NDE and SHM implementations are investigated. Glass fibers are selectively modified with nanomaterials with a deposition media in a screen printing process prior to the ply stacking of the fiber preform. Quasi-static monotonic tensile tests are used to characterize the damage initiation and damage sensing abilities of carbon nanotube

and xGnP based sensors. Progressive cyclic loading of specimens elucidate damage onset and accumulation behavior and aid in the development of quantitative methods to assess structural integrity.

Chapter 2

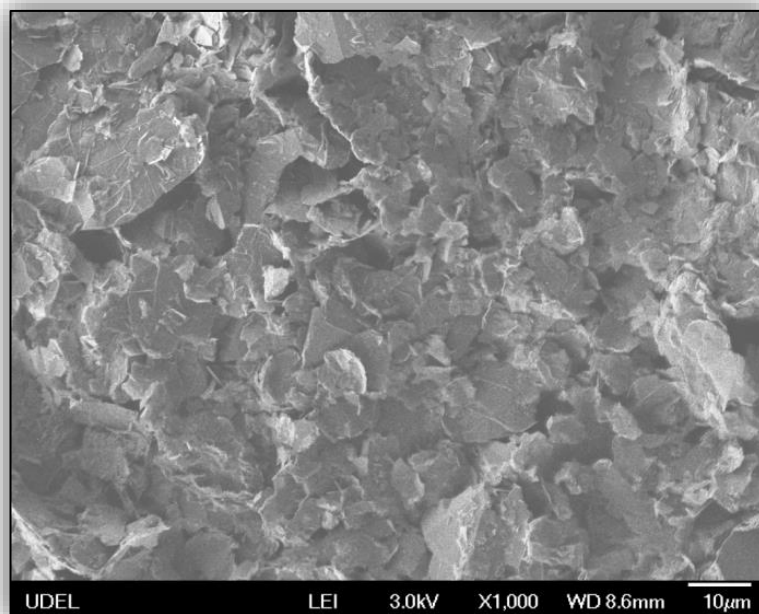
MATERIALS AND METHODS

2.1 Electrical Conductivity through Nano-Material Dispersion

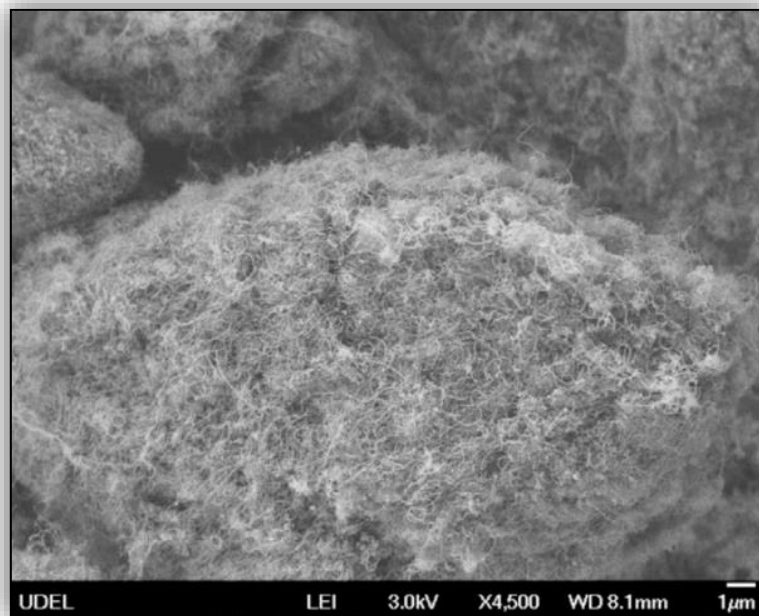
2.1.1 xGnP Nanocomposite

The graphene nano-platelets (xGnP m25, XG Sciences) are detailed by the manufacturer as consisting of a few layers of graphene in 25 μ m diameter particles [40]. The as-received nanoplatelets resemble graphite flakes with several layers, as shown in the SEM micrographs in Figure 2.1 (a). To fully realize the potential of the mechanical and electrical properties of graphene in the xGnP nanocomposite, methods to reduce graphite agglomerates to the desired few layers of graphene are required.

A shear intensive calendaring approach has been utilized in prior work for dispersing agglomerated carbon nanotubes [41] but the vastly different morphologies require specific processing regimes for graphite exfoliation. A thermosetting epoxy resin of diglycidyl ether of bisphenol F resin, (EPON 862, Momentive Specialty Chemicals Inc.) was prepared using a master-batch approach with five weight percent xGnP and used throughout this study. The epoxy and xGnP are initially hand mixed to wet all of the powdered nanomaterial to prevent subsequent material loss during handling.



(a)



(b)

Figure 2.1: Electron micrographs showing xGnP (a), and carbon nanotubes (b), in their as-received state. The difference in nanomaterial feature size is apparent in the difference scales for each micrograph.

The xGnP/resin mixture was then processed at successive gap settings of 100, 80, 60, 40 μm using a three-roll-mill (EXAKT 80E, EXAKT Technologies, Inc.) to determine which appropriate processing conditions the multifunctional response of the material. These gap settings are large in comparison to carbon nanotube processing, which goes down to gaps of 5 μm . Smaller gap settings, below 40 μm , were found to significantly degrade material electrical properties and are not included in this study.

2.1.2 Patterned Hybrid Nanocomposite

2.1.2.1 Patterning Media Synthesis

Hierarchically structured patterns are deposited onto fiber plies using an adapted screen printing method. The nano-enhanced patterning media was formulated specifically to serve as both a fiber sizing agent and a screen ink.

Water-based chemistry was selected over the commonly used screen ink of a PVC suspension in a plasticizing emulsion, or plastisol base, due to processing and adhesion concerns [42]. Another concern with PVC is its lower glass transition temperature than the epoxy matrix. Glass fiber sizing agents consist of water-based dispersions with emulsified polymers and coupling agents to promote adhesion at the fiber/matrix interface [43]. Additional processing constraints inherent to screen printing require modification of surface tension and viscosity to obtain an ink with desirable rheological properties.

A coalescing agent (PVP K-90, Ashland Inc.) was first added to ultra-pure water to ensure an even dispersion of the polymeric ink binder (Polyox WSR N-60k, Dow), which promotes adhesion of the deposition to the glass fibers. The binder is required to increase the ink's surface tension since the ultrapure water alone has a

surface energy (72 dynes/cm²) which exceeds that of the glass fiber substrate (46 dynes/cm²) and results in poor wetting of the fiber. The viscosity is adjusted with the hydroxyethyl cellulose water-soluble polymer (Cellosize QP 52000, Dow) to thicken and impart thixotropic behavior, a form of pseudo plasticity where a material's viscosity continues to decrease or 'thin out' during shearing. Shear thinning is an essential property for printing clear patterns with consistent thicknesses and substrate penetration. All of the rheological additives are added at a concentration of 1 wt. % of the water in the order they are presented.

2.1.2.2 Patterning Media and Nanomaterial Integration

Dispersion of the agglomerated as-received nanomaterials into the precursor solution is completed using a shear-intensive process. The highly dispersed nanomaterials provide the necessary electrical conductivity to form the sensor networks.

Chemical vapor deposition-grown multi-walled carbon nanotubes (CM-95, >95 % graphitic carbon, Hanwha Nanotech, Korea) and graphene nano-platelets are processed to reduce the agglomerated nanomaterials to the desired morphology in Figure 1.3. The several micron-long carbon nanotubes agglomerate into intertwined bundles, shown in Figure 2.1 (b), and are untangled by the calendaring approach while maintaining the desirable aspect ratio. The large aspect ratio enables electrical percolation at lower concentrations. Shearing of the xGnP turbostratic carbon planes into the idealized few layer graphene increases the effectiveness of its nanocomposites. The as-received powdered xGnP nanomaterial is added to the precursor solution and then processed using an intense shear mixing approach using a three-roll calendaring mill. The larger size of the xGnP requires processing at larger

gap settings to achieve an electrically conductive solution but requires less processing than carbon nanotubes, which requires processing at finer gap settings [44]. There exists a nonlinear relationship between the extent of carbon nanotube processing and electrical resistivity [45], where smaller gap settings create local maximum and minimum resistivity values indicating a transition from agglomerated particulate versus disentangled carbon nanotube dispersion.

Table 2.1: Processing parameters for patterning media

1 wt. % Carbon Nanotubes		5 wt. % m-25 Graphene	
Passes (#)	Gap Setting (μm)	Passes (#)	Gap Setting (μm)
5	20	5	100
5	15	5	80
5	10	5	60
20	5		

2.2 Composite Manufacture and Electrical Testing Preparation

2.2.1 xGnP Nanocomposite Tensile Bar

A curing agent or (part B) of the epoxy, is a non-ionic aqueous dispersion of Polyamine (EPIKURE W, Momentive Specialty Chemicals Inc.) and is added at a 100 to 26.4 weight ratio of the resin content of the post-milled material. Tensile bars are then cast into a steel mold coated with a release agent (Frekote 700-NC, Henkel Inc.) to produce specimens shown in Figure 2.2. Specimens are degassed in the mold at 60°C for two ten-minute intervals to remove voids produced when filling the mold. Copper strand is placed within the wet resin at each end of the composite to serve as electrical lead and is cured in place with the resin. The nanocomposites were then cured at 130°C for four hours.

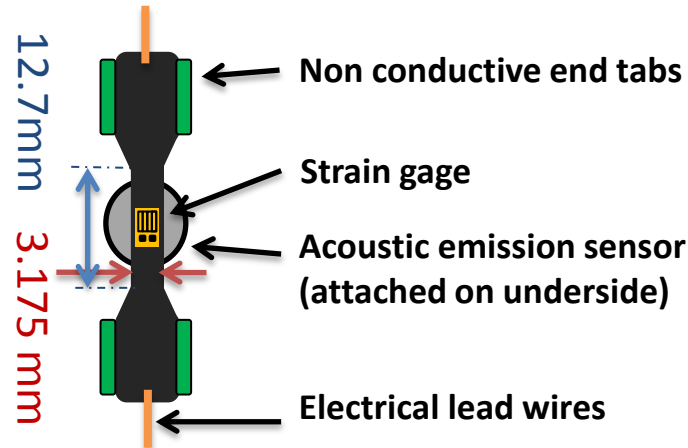


Figure 2.2: Illustration of nanocomposite tensile bar.

A reciprocating wet grinding wheel is used to remove the meniscus formed during casting and ensure a constant cross-section. Fiberglass material is then adhered to the end of the specimens to electrically isolate the nanocomposite from the load frame. Strain gages (Vishay CEA-00-UV250-350) are bonded to the specimen within the gage length using the manufacturer’s suggested practices [46]. Each batch of specimens processed to a gap size contained no less than six specimens and was reproduced twice in addition to a preliminary run of three specimens.

2.2.2 Patterned Sensor Composite

2.2.2.1 Adapted Screen Printing Process

The nano-media are directly deposited onto unidirectional E-glass in the desired pattern through use of an adapted screen printing process. A 120 count mesh is stretched to 18 to 22 Newtons and then coated with a UV-sensitive emulsion to form a stencil. A transparent plastic sheet with a high opacity image printed onto it is used to

shield the emulsion to prevent cure while the other regions of the stencil harden under the UV light. The uncured regions are then rinsed with water, exposing the bare mesh. The screen is then placed above the laminate in the 0° fiber direction. Application of the patterning media is directed through the mesh by hand at a consistent speed and pressure by in both forward and backwards directions twice to ensure a high quality print. After printing, laminates are heated at 60°C for four hours in a vented convention oven to expel the aqueous base of the precursor. Silver paint (SPI Flash-Dry™ Silver Paint, SPI Supplies) is then applied to the ends of the sensing region to serve as an electrical contact following resin infusion.

2.2.2.2 Composite Preparation

The patterned fiber ply is positioned atop the fiber preform, consisting of 4 layers of un-modified, unidirectional E-glass (13 oz./sq. yd., Jamestown Distributors) which is prepared for vacuum assisted resin transfer molding (VARTM) processing.

Unidirectional fiber composites with a 0° ply layup was selected to minimize the effects of resin rich regions that occur in woven fabric tow junctures and overlapping regions between orthogonally placed plies to enable a more precise study of the fiber-interface sensing capability. Vacuum pressure is used to infuse the preform with a commercial epoxy resin (EPON 862) with the aromatic amine curing agent (EPIKURE W), and is prepared at a 100 to 26.4 weight ratio. After curing at 130°C for four hours, the composite is machined to 12.7 mm (0.5 in.) wide specimens centered over the deposited sensor region.

The sensor's electrically conductive network is exposed through light sanding with 200 grit sandpaper. Silver paint is used to re-prime the entire sensor area for the electrical lead wire. A two-part silver-filled electrically conductive bisphenol-A-

(epichlorhydrin) epoxy (Epoxies, etc.) at a 1 to 1 weight ratio adheres the wire to the sensing area. Electrical isolation from the load frame is achieved through the addition of fiberglass end tabs bonded at a gage length of 76.2 mm (3.0 in), shown in Figure 2.3.

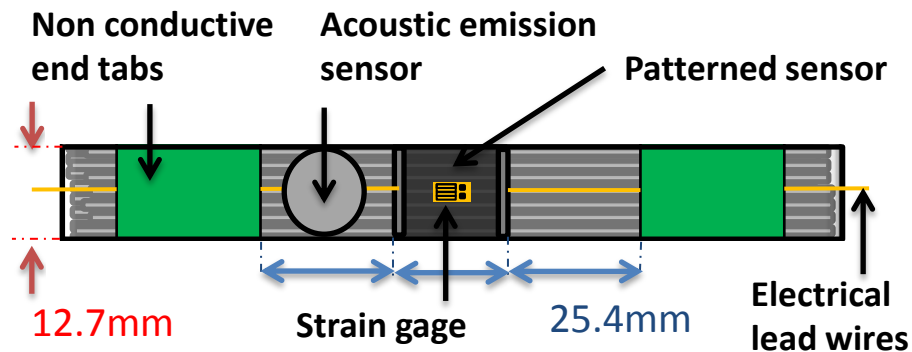


Figure 2.3: Illustration of a tensile bar with a patterned sensor.

2.3 Coupled Mechanical, Electrical, and Acoustic Characterization

A screw driven, displacement controlled load frame (Instron 5565/5567, 5/ 30 kN load cell for nanocomposite tensile bar/patterned composite) is used to perform quasi-static monotonic and progressively increasing cyclic tensile loading tests at a rate of 1.27 mm/min (0.5 in/min). Progressively increasing cyclic testing consisted of loading to 1 kN, unloading, then repeating while increasing by one kN until failure. Electrical resistance information is acquired using a NI PXI 4071 digital multimeter card with a 5.5 digit resolution. Strain data is collected with the NI PXI 4330 strain bridge card; the strain gage is adhered following the manufacturer's instructions and positioned in the center of the sensor on the tool side of the composite. Load data is acquired with the NI PXI 4300 analog card. A LabVIEW .vi is used to compile

resistance, strain, and loading data for real-time analysis. Additional hardware and software details are contained in Appendix A.

Elastic energy not consumed by the creation of new fracture surfaces releases stress waves that are measured as acoustic emissions with a sensor affixed to the surface of the composite and acquired using software from the manufacturer (Physical Acoustics, Princeton Junction NJ).

Final preparations are taken to record specimen performance and prevent specimen waste due to improper testing. Specimens are labeled in an alphanumeric system to reflect manufacture date; testing order, and nanomaterial content and concentration. Cross sectional areas of the specimens are measured to normalize the load across each test by calculating the stress in the material. Baseline strain values are used to null the strain gage to get an accurate measure of strain in the material. The undamaged resistance value R_0 is recorded prior to specimen insertion into the load frame grips and after tightening the grips to secure the specimen to ensure electrical isolation between specimen and frame.

The initial setup for the load frame involves calibrating the load cell, compliance testing, and verification of communication between load frame and data acquisition system. With successful specimen manufacture and testing, results can be analyzed to assess the material's damage sensing capabilities.

2.4 Summary

Material processing for carbon nanotube and xGnP self-sensing nanocomposites is detailed. Higher process efficiency is achieved using xGnP due to the reduced milling time required for preparing electrically conductive dispersions.

Chapter 3

xGnP NANOCOMPOSITE PROCESSING FOR SELF-SENSING APPLICATIONS

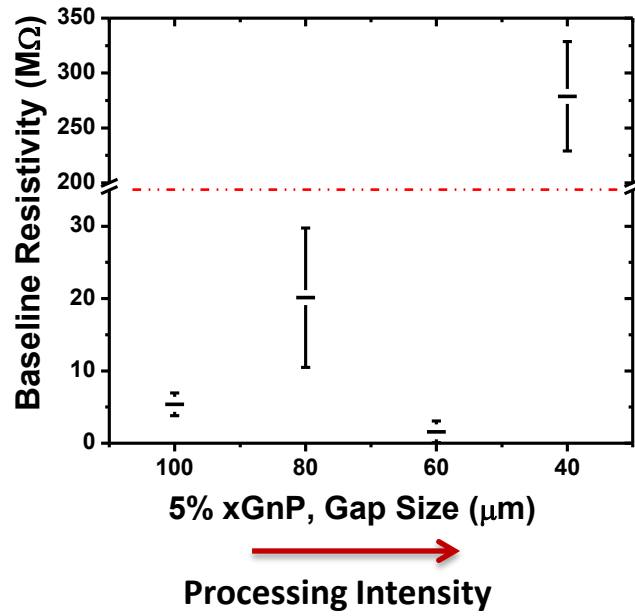
3.1 Introduction

xGnP nanocomposites are studied to determine processing conditions required to produce a piezoresistive response suitable for use in a damage sensing system. *In situ* damage sensing has been established with carbon nanotubes which create electrically conductive networks at low volume concentrations due to the material's high aspect ratio. xGnP potentially can serve as a low-cost alternative nanomaterial relative to carbon nanotubes for the creation of damage sensing networks.

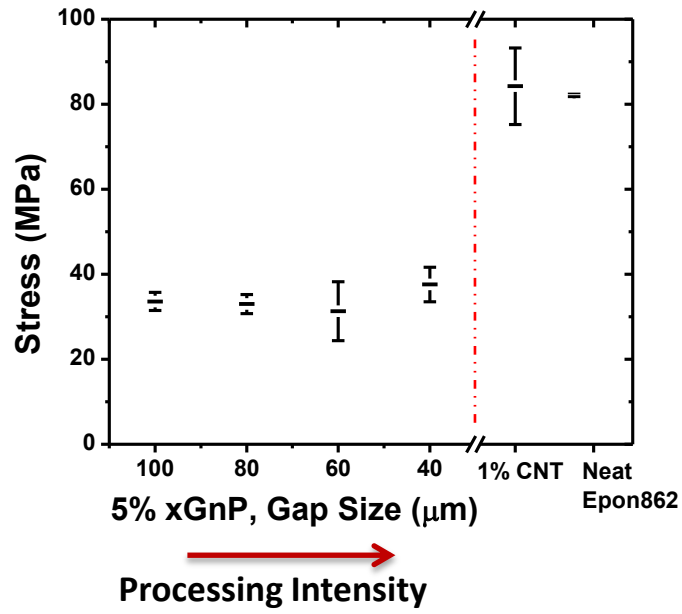
A shear intensive calendaring process is used to disperse and exfoliate the as-received xGnP material. Processed material is removed from the calendaring mill upon completion of a predetermined routine to study the relationship between processing intensity and piezoresistive response. Mechanical testing of the nanocomposite tensile bars has shown that each processing routine produces a characteristic piezoresistive response and gage factor.

3.2 Assessment of Multifunctional Performance

Tensile bars of xGnP nanocomposites processed using different parameters are tested under quasi-static monotonic tension to establish their resistance-strain relationship and to evaluate their mechanical properties to understand multifunctionality.



a)

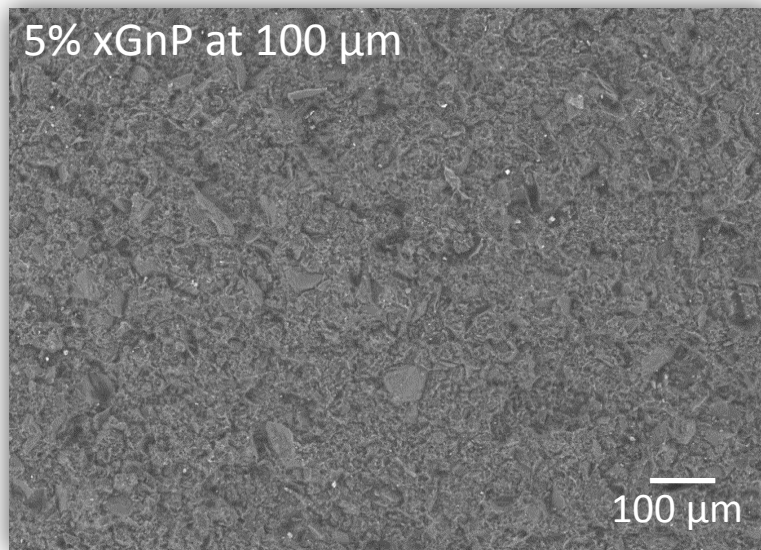


b)

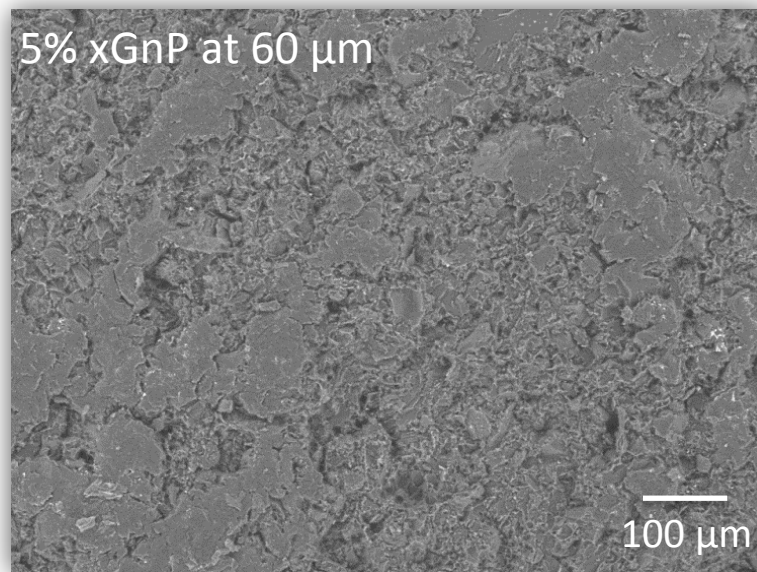
Figure 3.1: Processing intensity effects on xGnP: (a) resistivity and (b) strength at the different processing intervals.

The electrical property results presented Figure 3.1 (a) show that, with even minimal processing at a gap setting of 100 μm , the calendering approach is effective in shearing the graphite into smaller platelets (Figure 3.2 (a)) and forming electrical networks. The subsequent processing interval at 80 μm serves an intermediary step where the electrical resistivity increases. Processing at 80 μm reduces the particle size with limited new exfoliation of the layers, as shown in Figure 3.3 (a). The specimens processed at a gap setting of 60 μm yielded the lowest resistivity and is explained by the presence of spanning xGnP clusters (Figure 3.2 (b)). The micrographs in Figure 3.3 (b) show that the 40 μm xGnP is significantly degraded causing the resistivity to increase by two orders of magnitude. Continued processing at 20, 15, 10, and 5 μm yielded no further improvement. In Figure 3.1 (b) the reduction of tensile strength of the matrix is due to the high volume fraction of the xGnP particles, which shear easily along their inter-planar dimensions, creating stress concentrations that initiate failure at lower loadings (Figure 3.4). A similar local minimum values with larger gap settings are also found in carbon nanotube dispersions [42].

For damage sensing purposes, measuring the change in resistance from an established baseline (ΔR) alone is insufficient to assess the extent of damage. Normalizing the ΔR to the baseline produces a means for evaluation that can be applied to specimens of different resistivity. Quantitative analysis of the resistance data is performed using the percent change of the normalized difference from the baseline resistance value, $\Delta R/R_0$ (%). Qualitatively, we understand the resistance change to result from the change in contact resistance due to the changes in tunneling gaps between nanoparticles, which serve as electrically conductive pathways during direct current resistance measurements.

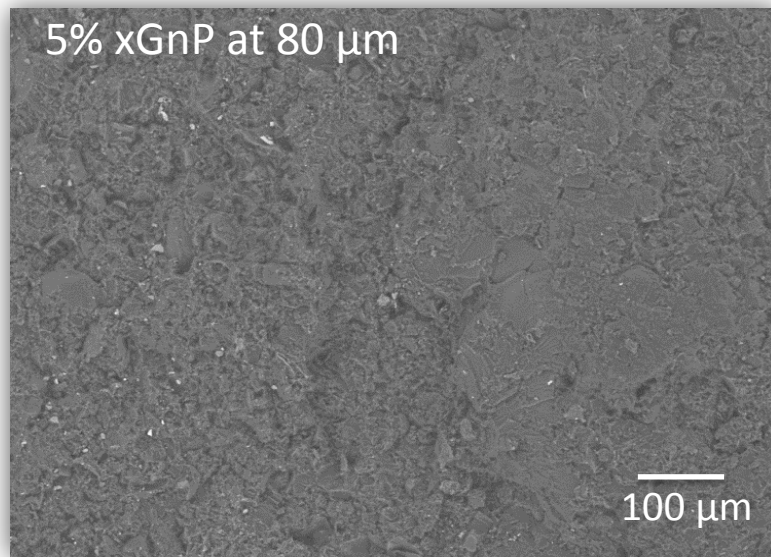


a)

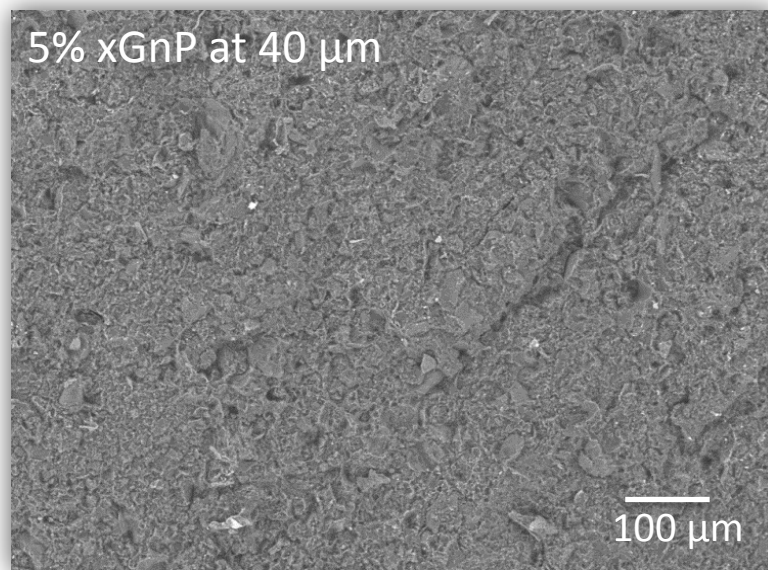


b)

Figure 3.2: Electron micrographs of a fracture surface. (a) Material processed at a 100 μm gap showing the platelets well dispersed throughout the matrix. Thermodynamic instability due to the xGnP particle dispersion in a polar matrix material leads to the re-agglomeration of xGnP into clusters. (b) Clusters shown in materials processed at a 60 μm gap setting are found throughout the nanocomposite and form the electrically conductive network.



a)



b)

Figure 3.3: Electron micrographs of a fracture surfaces of the xGnP nanocomposites. (a) Nanocomposites processed at a 80 μm gap shows numerous large platelets. The thermodynamic instability produces only a few clusters, reducing the overall electrical conductivity. (b) Material processed at gap settings of 40 μm showing a highly textured fracture surface, with smaller platelets sparsely distributed. Few xGnP particles remain intact, explaining the low conductivity of the nanomaterial.

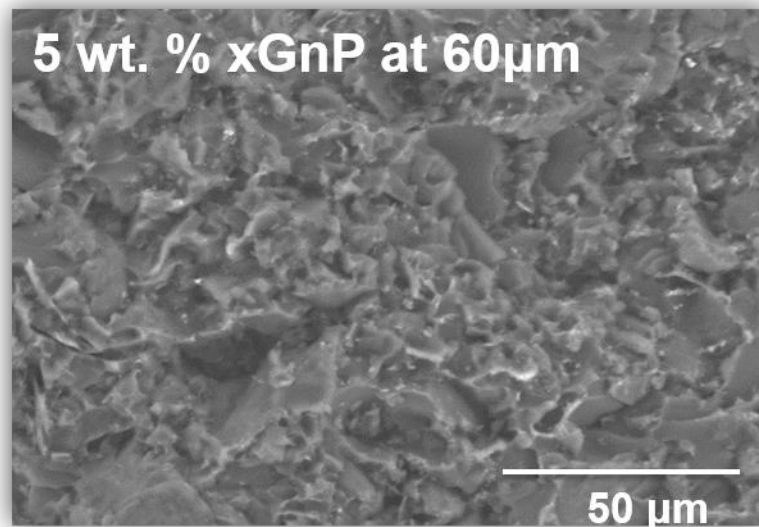
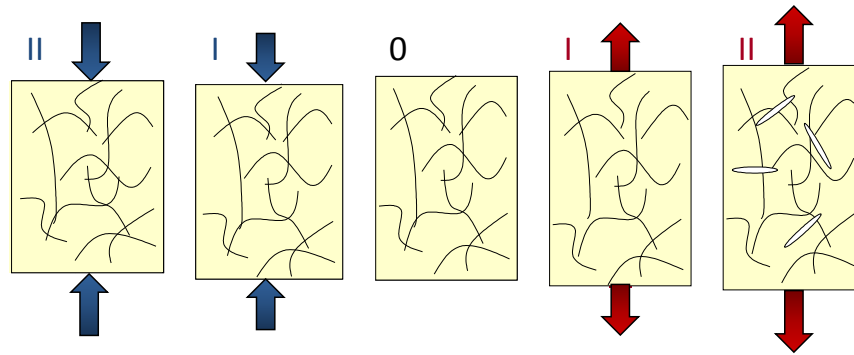
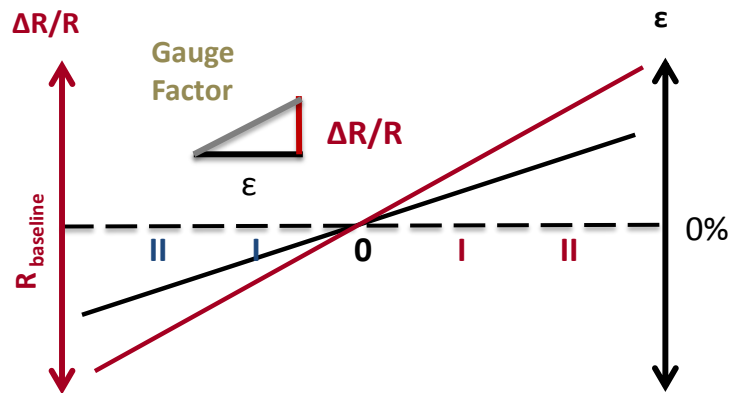


Figure 3.4: Electron micrograph showing xGnP oriented perpendicular to the fracture surface, indicating that the platelets act as defects where the crack propagated. xGnP aligned parallel to the fracture surface is not visible. Their adhesion between the exterior basal planes and matrix exceeds the strength of perpendicular aligned plates, whose strength is dominated by inter-planar shear strength.

This piezoresistive effect of the xGnP network is evident in both tension and compression, as illustrated in Figure 3.5 (a). The gage factor is used to measure the coupling of mechanical and electrical properties based on the slope of normalized resistance change and strain, as shown in Figure 3.5 (b).



a)



b)

Figure 3.5: (a) Piezoresistivity illustration of effects on carbon nanotube dispersion conductive pathways subjected to compressive, zero, and tensile strains and the associated (b) resistance-strain response.

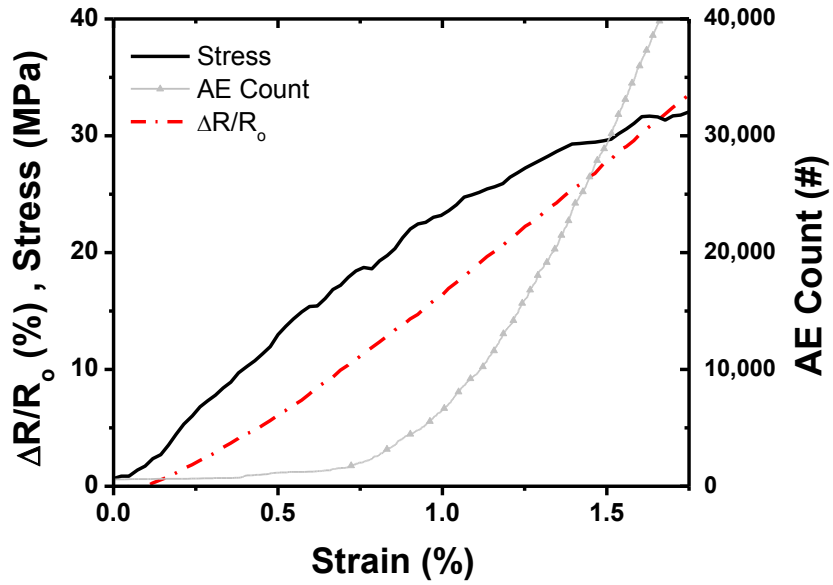
Acoustic emission (AE) is a conventional sensing tool which complements the electrical sensing by providing an additional tool through which the formation of damage mechanism can be validated. AE sensors register the release of energy, or stress wave propagations, from micro-crack initiation and growth. Cumulative AE counts are widely used as a qualitative measure to assess the formation of damage. AE requires active monitoring at all times. In contrast, the *in situ* method relies upon the

material's resistance, permitting intermittent, low-power sensing. Experimentally, the ability to relate AE events with distinct resistance behavior enables the characterization of the xGnP sensing response to study the extent of damage and aids in the development of tools capable of quantifying the material's structural integrity.

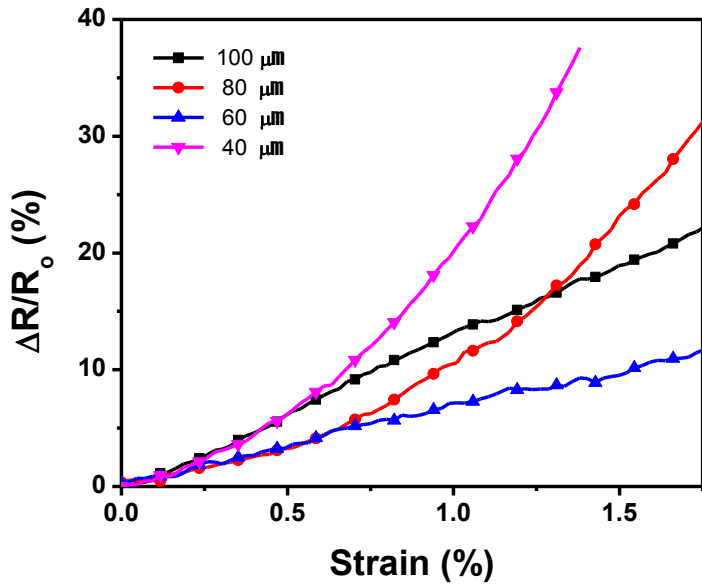
The plot in Figure 3.6 (a) is a representative tensile test in which the nanocomposite is loaded until failure. At 0.60 % strain, the resistance signal slope changes, indicating an increase in gage factor and the AE total begins registering hits at a progressively increasing rate. AE at this low strain level are not reflected in the resistance response, suggesting no damage is sustained to the electrical network. The fracture of the xGnP platelets along the planar direction would not significantly affect the resistance response and the released strain energy is recorded as AE hits.

The average resistance response for each type of specimen in Figure 3.6 (b) shows that the material processed at 100 and 60 μm act as integrated strain sensors with a constant gage factor, as defined in Figure 3.5 (b). Gage factor can be interpreted as a measure of strain sensitivity and must be well-defined for a material for use in sensing applications. The inconsistent behavior and nonlinear resistance-strain response for the 80 and 40 μm samples results from their higher electrical resistivity and less favorable morphologies shown in Figures 3.3 (a) and (b).

Processing the xGnP nanocomposite down to a gap setting 60 μm was chosen because of its consistent gage factor and lower initial resistance. The specimens processed at 100 μm demonstrated similar performance with a higher gage factor but display a higher initial resistivity. This could result in specimens having measured



a)



b)

Figure 3.6: (a) Typical stress, normalized resistance- strain loading curve of 60 μm .
 (b) Processing intensity effects on gage factor.

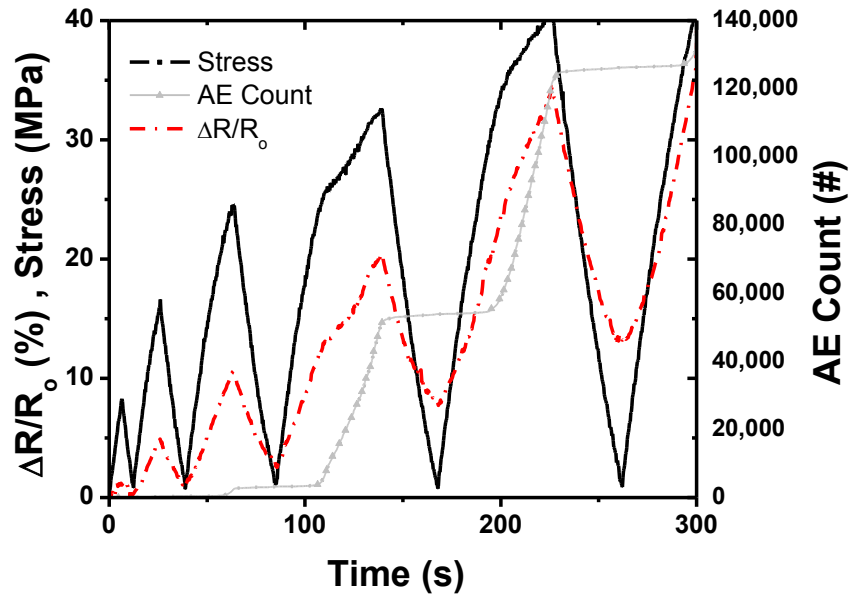
resistance above the 6 G Ω range, which is the upper limit on most digital multi-meters. As a result the 100 μm specimens would require more expensive data acquisition equipment.

3.3 Damage Onset and Propagation

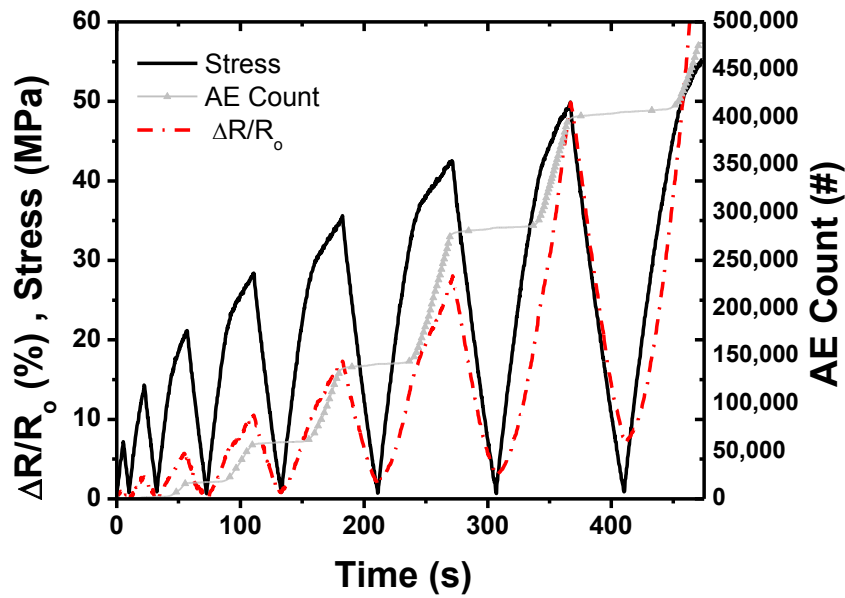
Prior work has established that damage progression in fiber reinforced nanocomposites can be observed through cyclic loading of increased magnitude, enabling the observation of micro-crack opening and closing. The high aspect ratio of carbon nanotubes results in a non-invasive conductive network that penetrates fiber bundles and spans the interlaminar region between plies. The change in nano-additive geometry requires evaluation of the xGnP nanocomposite response for characterizing damage onset and propagation behavior.

The first three load cycles (Figure 3.7 (a) and (b)) are within the material elastic limit, producing no damage. Minimal deviation from the resistance baseline is observed and the AE total is negligible. An expanded view of the later cycles, presented in Figure 3.8, illustrates the interrelationship of material response as detailed by stress, resistance, and AE count data. The vertical dashed lines (Figure 3.8) at the knee and apex of each stress curve are closely matched by responses in the AE and resistance curves.

The slope of the upper section of the knee on the stress curve decreases with passing cycles indicating a decrease in the material's elastic modulus, resulting from new damage (i.e. separation of xGnP platelets). Over this time interval, the AE response completes another step-like increment, while the resistance signal demonstrates nonlinear behavior. Upon conclusion of the cycle, the baseline resistance, taken at zero load, increased and reflects damage initiation.



a)



b)

Figure 3.7: Transient resistance change and AE cumulative counts during progressive cyclic loading with materials processed at (a) 100 μm , and (b) 60 μm .

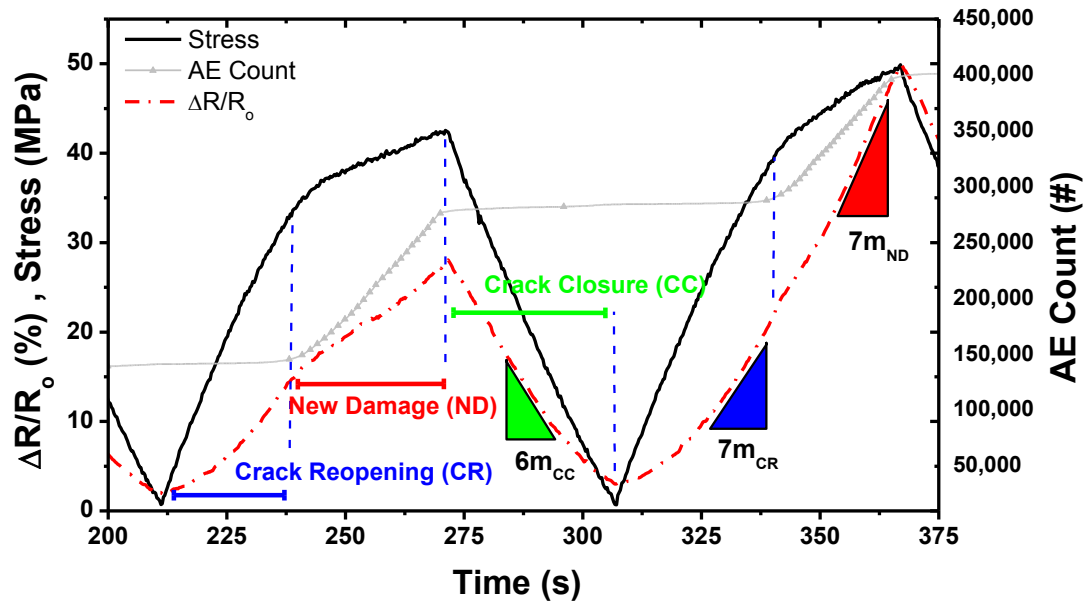


Figure 3.8: Damage-sustaining cycle illustrated to define relevant terms and parameters of the resistance signal. Elastic response and crack reopening are associated with the first part of the resistance response. Beyond the knee in the resistance response, new damage is incurred where the xGNP layers separate. During unloading the cracks that opened during loading close.

Observation of the resistance response with consideration of stress and acoustic data sheds light on the mechanisms present in the nonlinear loading resistance behavior, shown in Figure 3.8. The nonlinear resistance during loading reflects crack reopening and elastic deformation during the first region. The deviation of the resistance signal from the initial linear response at the knee directly correlates with a decrease in stiffness in Figure 3.9 and an increase of accumulated AE hits.

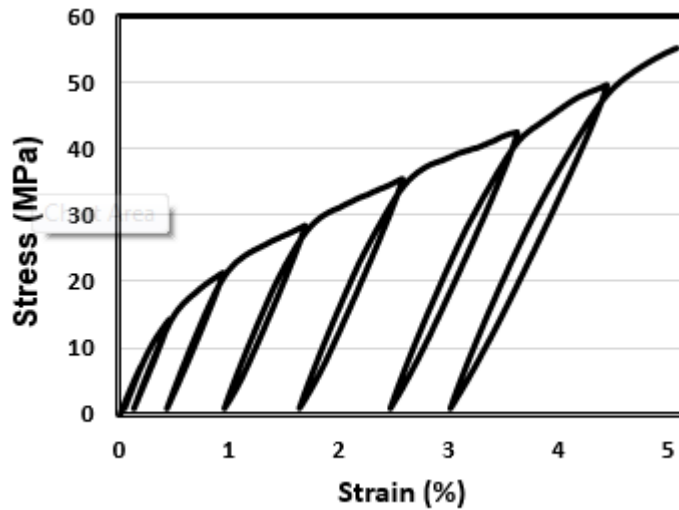
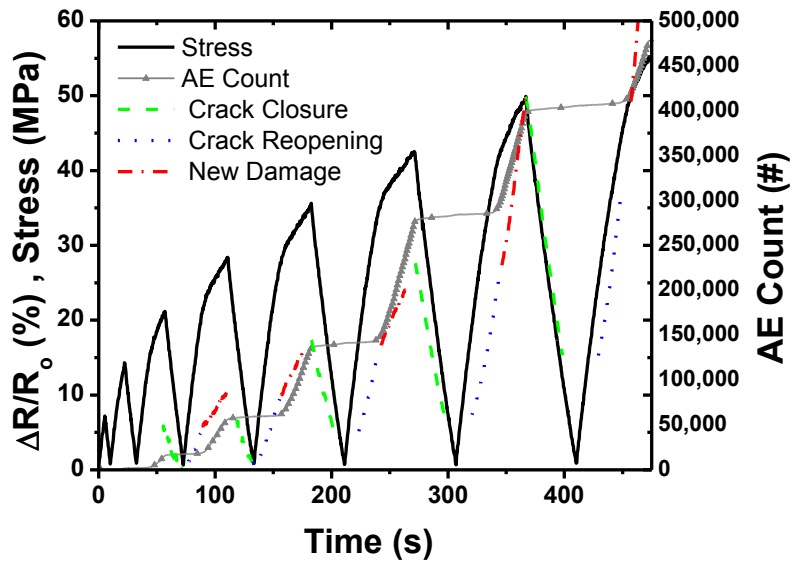
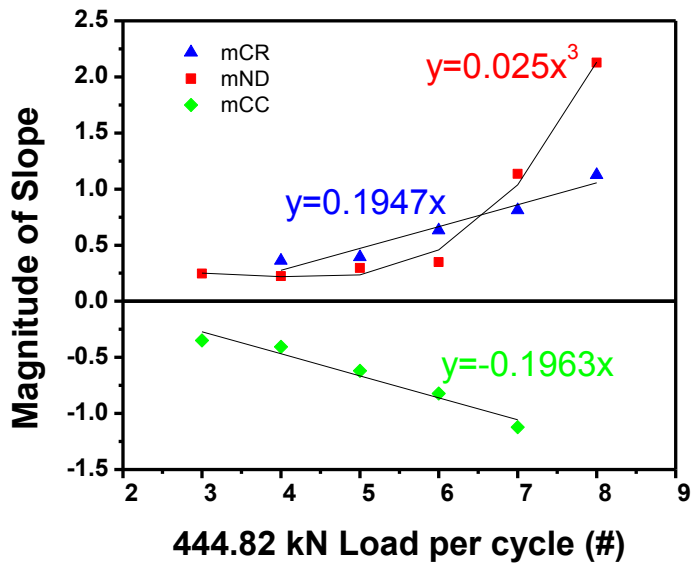


Figure 3.9: Stress-strain plot showing stiffness loss after the second cycle.

This suggests that the initial resistance slope is associated with the specimen elastic response followed by the reopening of micro-scale cracks from prior damage events and is identified as crack reopening (CR). At the knee in the resistance curve, each successive load initiates a new damage (ND) region at the prior cycle's maximum load suggesting the earlier separations of xGnP planes have reopened to and are now propagating. The first damage region initiates around 25 MPa, as seen in Figure 3.7 (a) (b). The increase in the slope (m_{ND}), as shown in Figure 3.10 (a), at higher load cycles becomes more pronounced and can serve as a warning of impending failure. It is approximated by a least-squares cubic fit (Figure 3.10 (b)). The volatile nature of the cubic growth in the slope of the ND curve renders this measure a poor indicator for predicting failure and assessing a structure's health.



a)



b)

Figure 3.10: (a) Regional assignment for crack reopening (CR), new damage (ND), and crack closure (CC), and (b) curve fits from each region during load cycles, increasing by 444.82N per cycle.

The crack reopening progression has a linear behavior, making it a preferred parameter for damage assessment. It has limited utility in application due to its nature as a lagging indicator. In a real-time SHM application, the ability to observe that an indicator has just reached or surpassed a critical value may be too late to prevent new damage, or worse, an uncontrolled failure event. A leading indicator in a SHM sensor response would provide actionable feedback prior to the beginning of an activity that could compromise the material, thus ensuring the structure performs within a safe operating envelope.

The crack closure (CC) response during load removal is a featureless, linear response, with slope m_{CC} . Observation of the CC and CR regions in Figure 3.8 (a) shows that the two slopes appear as mirror images of each other. This reinforces the assertion that the first regime corresponds to reopening of existing damage, as it matches the behavior of crack closure while the applied load is removed. Utilizing the linear least-squares method to approximate slope, plotted in Figure 3.10 (b), it is apparent that $|m_{CC}| \cong |m_{CR}|$. This direct correlation between the CC and CR response establishes m_{CC} as a viable means for damage sensing, since it serves as a leading indicator capable of assessing the likelihood of failure prior to the beginning of a damaging event.

In terms of the gage factor response of different regions, the time domain and strain domain can be considered equivalent since the load frame is operating at a constant crosshead displacement rate. The CR and CC region can be understood as the response of a material that is deforming under loads it has already experienced. The ND gage factor correlates to the response of the specimen to higher loads not yet

experienced by the sensor. This strain-memory related behavior can be utilized in different applications to assess the extent of damage to predict material failure.

3.4 Real-Time Damage Response

Monitoring the electrical properties of a material in an unstressed or predefined state for comparison with a baseline value is a well-established practice for any electrical-phenomena-based sensing. The piezoresistive nature inherent to the nanocomposite structure renders this sensor type vulnerable to inaccurate readings precipitated by the inability to repeat the loading conditions from the baseline reading. Unexpected internal stresses can develop in load-bearing structures due to improper component assembly or damage to sub-assemblies connected to the self-sensing component over its service life. NDE and SHM methods rely upon comparison of signals from a static, unloaded state to establish a baseline, with subsequent measurements taken throughout the component's use. Without physically isolating a component containing a self-sensing material, or precisely replicating the loads at which the baseline measurement were taken, the loading state at the time of measurement will influence the resistance measurement. A small, unaccounted for, compressive or tensile force applied to the structure during testing will produce a reading that is either under or over the actual baseline, as illustrated in Figure 3.5 (a). Consequently, relying upon the static nature of the baseline technique, alone, can produce inconsistent readings, providing an inaccurate assessment of damage within the material.

Real-time correlation of the rate of change for the resistance response and the loading rate has the potential to serve as an additional technique to assess the relative health of a composite irrespective of loading conditions. Opportunity exists to develop

an NDE procedure where a repeatable means to direct a controlled input or stimulus to a sensing material to gather the respondent resistance signal. The magnitude of the load would have to be such that the composite sustains no damage, and produces a resistance signal within the range of the well-defined elastic response and crack reopening region. Analysis of this slope, and the progression of its change over the material's life is a suitable means by which to determine the overall health of the composite in addition to the baseline approach.

3.5 Summary

This research has shown xGnP can serve as a nano-additive for resistance based damage sensing methods. Prior research has established carbon nanotubes in this role and explored the processing relationship between electrical resistivity and processing intensity as influenced by the gap setting on a calendering mill. Similar characterization of xGnP has expanded upon this work to consider the sensor gage factor at different processing intensities. Processing at a 60 μm gap was found to produce nanocomposites with the lowest resistivity and a linear gage factor.

Damage at low strain levels are the result of xGnP flakes separating or shearing along their inter-planar direction which reduces the ultimate strength of the nanocomposite. During loading and unloading cycles, the nonlinear resistance response of the xGnP nanocomposite is used to study the damage progression. The onset of damage and its progression can be analyzed using an SHM approach that considers the rate at which slopes of the crack reopening, new damage, and crack closure resistance response change occur. Application of this time-dependent resistance behavior and gage factor response of the material under known loading can be used as a real-time damage sensor.

Chapter 4

HIERARCHICAL PATTERNING FOR *IN SITU* INTERFACIAL SENSING

4.1 Introduction

Damage sensing in composites through incorporating networks of carbon nanotubes has proven effective for measuring the initiation and progression of multiple types of damage. Current approaches for nanotube-based damage sensing rely on modifying the entire composite structure, allowing for distributed resistance based damage sensing. Costs associated with manufacturing nanocomposites for self-sensing of large structures could become prohibitively expensive. An alternative approach is to selectively place integrated sensors in regions prone to failure. A controlled network of sensors has potential to be streamlined into a multi-scale damage monitoring system for NDE or SHM applications.

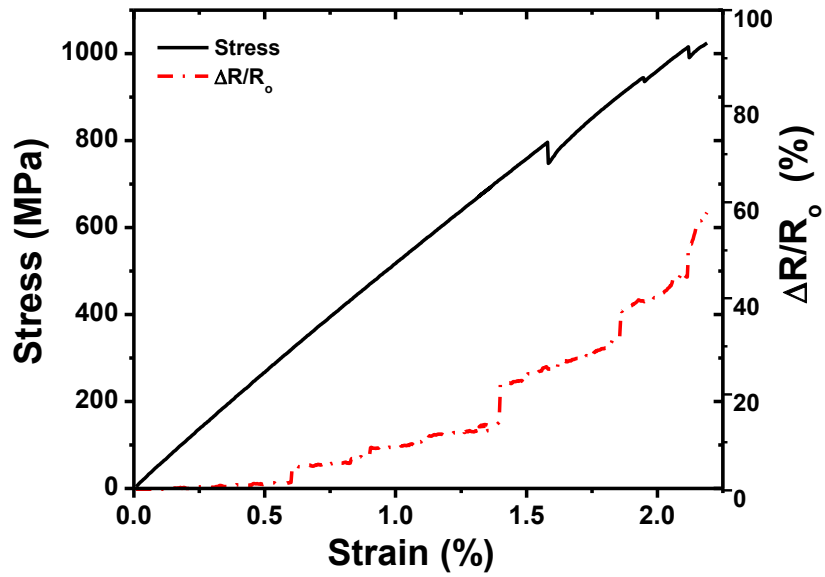
In this chapter, a method to selectively pattern nanomaterials onto fibers for damage sensing is detailed. The manufacturing technique deposits a limited amount of nanomaterial onto the fiber, creating a sensor designed to monitor damage at the matrix and fiber interface region. The damage onset and progression behavior is explored for carbon nanotube and xGnP based sensors.

4.2 Quasi-Static Tensile Tests

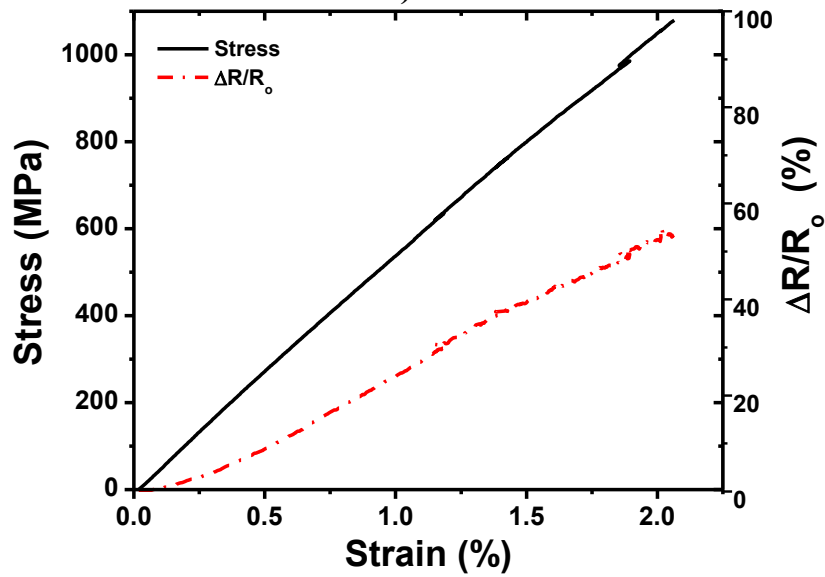
Tensile tests are performed to determine how the composition of nano-scaled carbon allotropes affect the piezoresistive response of the patterned sensors. The resistance response reflects the extent of damage to the electrically-conductive network deposited onto glass fabric. The statistical nature of fiber fracture results in complex damage initiation and progression, where the extent and location of fiber and matrix failures varies from part-to-part.

The carbon nanotube and xGnP sensors' piezoresistive response (Figures 4.1 (a) and (b)) show characteristic behavior resulting from the different geometries and size of the nano-scale additives. The carbon nanotube sensing response shows step-like increases in resistance, where the steps correspond to fibers being fractured and the supported load redistributed via shear in the polymer matrix at the location of fracture. The slope between steps corresponds to the extension-induced piezoresistive response of the carbon nanotube network and their slope progressively increases to reflect the decreasing number of conductive pathways. The deposition of conductive materials on the surface on the non-conductive fibers enables the detection of first fiber fracture. This is in contrast to the response where carbon nanotubes are uniformly distributed throughout the polymer matrix.

As shown in Figure 4.1 (b), the xGnP sensors lack the ability to register local damage sensing events but act as a global strain sensor with a constant gage factor. The sensitivity of the xGnP electrical response decreases throughout the load cycle and is believed to be the result of the shearing apart of larger graphite flakes, increasing the signal-to-noise ratio of the sensor system.



a)



b)

Figure 4.1: Characteristic responses of patterned (a) carbon nanotube and (b) xGnP sensors.

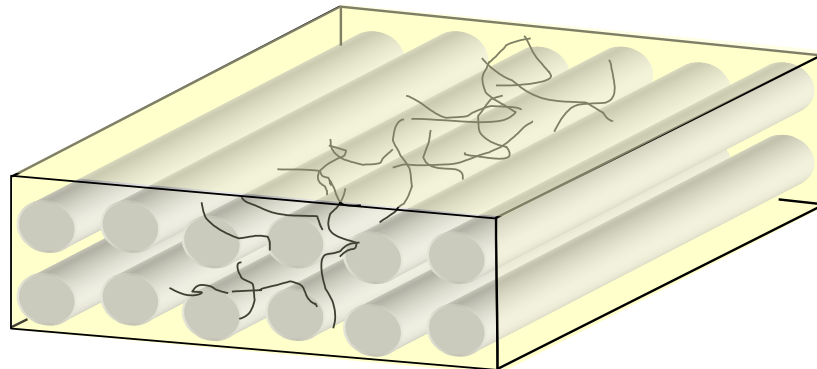
The response of the patterned carbon nanotube sensor demonstrates the effectiveness of interface-based sensing by advancing the capabilities of *in situ* methods to offer insight on fiber fracture events. Similar unidirectional composites were studied by Thostenson *et al.* [10], where a matrix modified with carbon nanotubes throughout the composite produced a linear resistance-strain curve up to failure. The extensive network of carbon nanotubes throughout the matrix provided a sufficient number of electrical pathways and did not detect individual fiber fracture events. The response observed was similar to the performance of the xGnP sensor.

Consideration of the strain response provides additional insight to identify the initiation of damage. The representative carbon nanotube specimens have a featureless, linear response up to 0.60 % strain, indicating no permanent damage is sustained prior to that critical strain value. Above 0.60 % strain, step-like jumps in the resistance occur, corresponding to first fiber fracture. The xGnP sensor is unable to distinguish between elastic deformation and the onset of damage.

Observation of the optical micrographs in Figures 4.2 (a) and 4.3 (a) helps elucidate the difference in damage versus strain sensing between the carbon nanotubes and xGnP patterned sensors. The carbon nanotube deposition shows that the material is well dispersed across the fabric and penetrates the fiber bundles to form an electrically conductive, non-invasive *in situ* network. Preferential formation of conducting pathways by the carbon nanotubes along the fiber direction is expected during manufacture [44]. The xGnP deposition does not penetrate the fiber bundles and creates the electrically conductive network on the fabric surface with minimal penetration with reduced sensitivity compared to the carbon nanotube sensor. Illustrations of the microstructure are shown in Figure 4.2 (b) and Figure 4.3 (b).

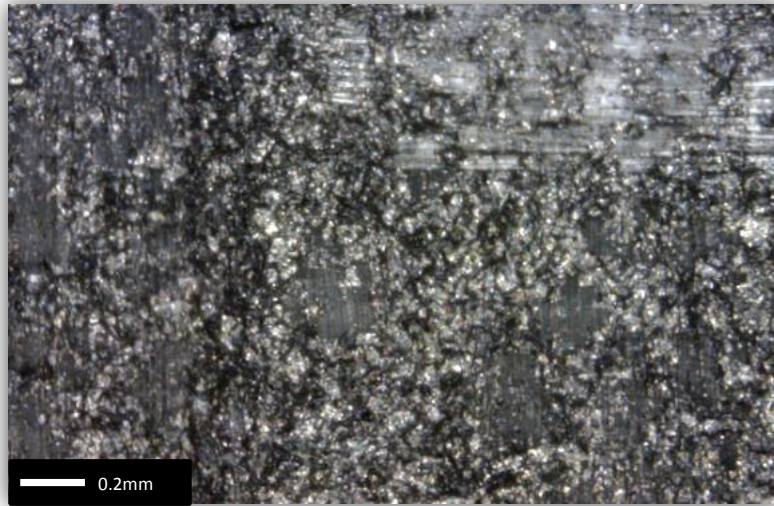


a)

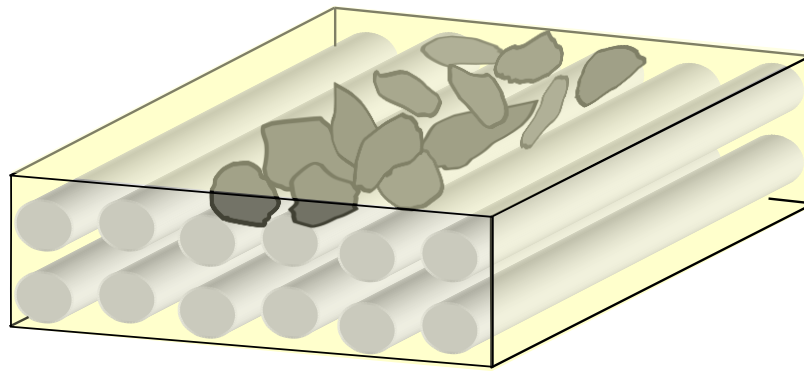


b)

Figure 4.2: Optical micrograph of carbon nanotube (a) onto glass fibers showing the coverage and distribution of material and illustration (b).



a)



b)

Figure 4.3: Optical micrograph of xGnP (a) on glass fibers showing the coverage and distribution of material and illustration (b).

Lower xGnP baseline resistance values are the result of a higher concentration of conductive nanomaterial being confined to a limited space on top of the fabric. The carbon nanotubes, which penetrate the fiber bundles, create fewer conductive pathways at the same reinforcement content. The sensitivity range, summarized in Table 4.1, is a measure of the change of baseline to failure resistance and can be used, in conjunction with the sensor gage factor, to predict at what resistance value the specimen will fail. The carbon nanotubes demonstrate a wider range in resistance, with a $26 \pm 13\%$ increase from the baseline to failure. Here, the nanotubes detect the accumulation of fiber. The step-wise response of resistance-strain due to the ability to sense fiber damage complicates calculation of the sensor's gage factor beyond first fiber fracture. The xGnP sensor allows for accurate strain prediction due to its linear gage factor and displays a well-defined sensitivity range of $74 \pm 8.4\%$.

Table 4.1: Carbon nanotube & xGnP mechanical and electrical properties

	Strength (MPa)	Critical Strain (%)	Baseline Resistance (kΩ)	Sensitivity Range (%)
xGnP	1061.7 ± 7.8	N/A	14.8 ± 8.4	74.5 ± 15.8
CNT	999.1 ± 22.1	0.60	45.8 ± 2.5	26.1 ± 13.2

The sensitivity range can be utilized as a method to process sensor data for predicting material failure. With the baseline resistance and empirical values for the sensitivity range, one can formulate failure probability of the structure at a measured resistance change from its baseline value, ΔR .

$$P_f(\Delta R) = \frac{\Delta R}{R_{Baseline} * \left(\frac{\phi_{Sensitivity Range}}{100} \right)}$$

Understanding the monotonic tensile response serves as a foundation to build knowledge of a specific composite's failure mechanism. Structures typically fail from the accumulation of micro-scale damage as opposed to loads exceeding the design limit. Damage progression information is required for NDE and SHM applications, so loading conditions reflecting real world conditions must be applied.

4.3 Transient Damage Sensing Response

Figures 4.4 (a) and 4.5 (a) show the transient resistance response during progressive cyclic loading for each sensor, indicating different behavior at the baseline values between cycles. The carbon nanotube resistance signal return to their initial value upon completion of its first three cycles and indicates that sensor is loaded within its elastic limit. No such elastic recovery in the sensor electrical conductivity is visible for the xGnP sample, with a deviation in the baseline value after the first cycle is completed. The increase in noise for the xGnP electrical signal near failure is observed in the monotonic tensile loading (Figure 4.1 (b)) and is more visible in Figure 4.5 (a). This behavior presents an opportunity to monitor structural health by measuring the increase in signal to noise ratio.

The resistance- strain response is well established in prior work as a quantitative tool to study and track damage accumulation in carbon nanotube-based composites. In Figure 4.4 (b) the critical strain value of 0.55% corresponds directly with a knee behavior in the resistance curve during the loading of the 4th cycle. After this level of strain, permanent damage is sustained and is visible along the resistance axis at zero strain. This early detection of damage is associated with the failure of the weakest fibers and is consistent with the high variability of fiber strength.

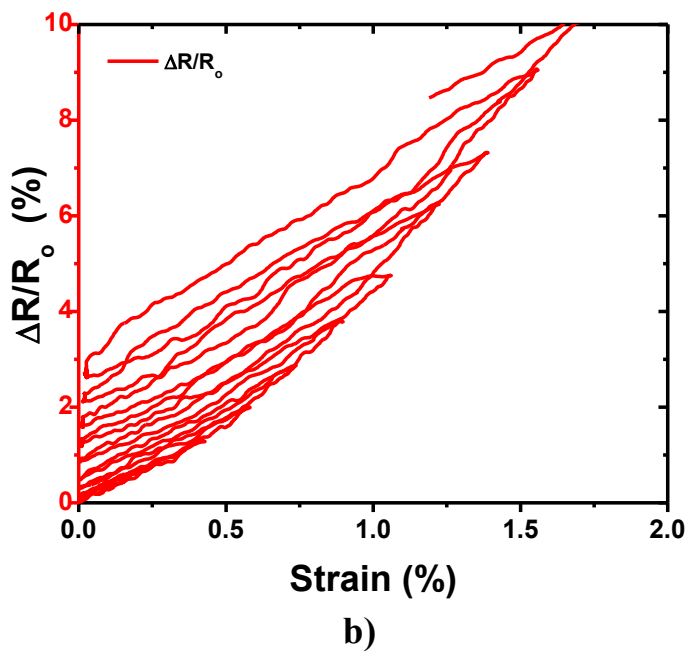
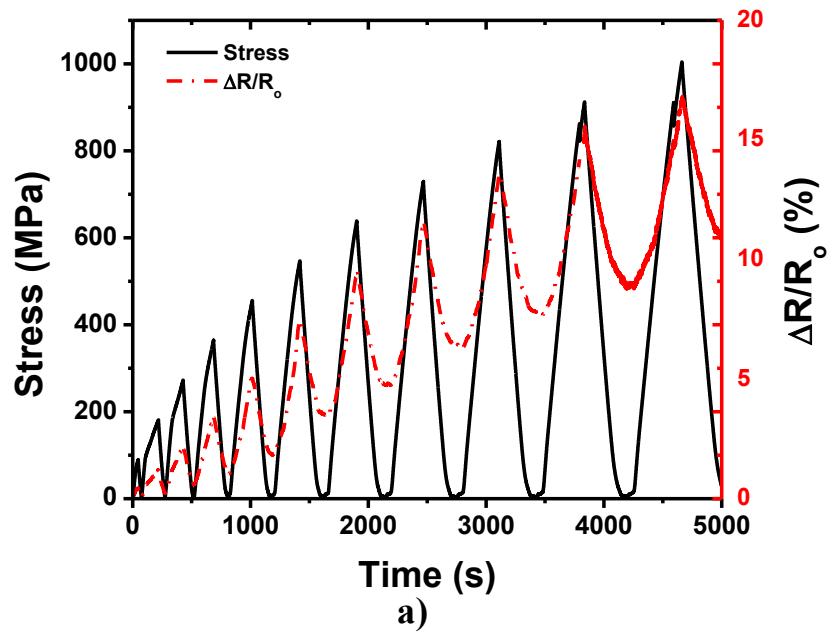


Figure 4.4: (a) Cyclic loading-displacement-resistance plots for carbon nanotube sensor and (b) resistance-strain plot.

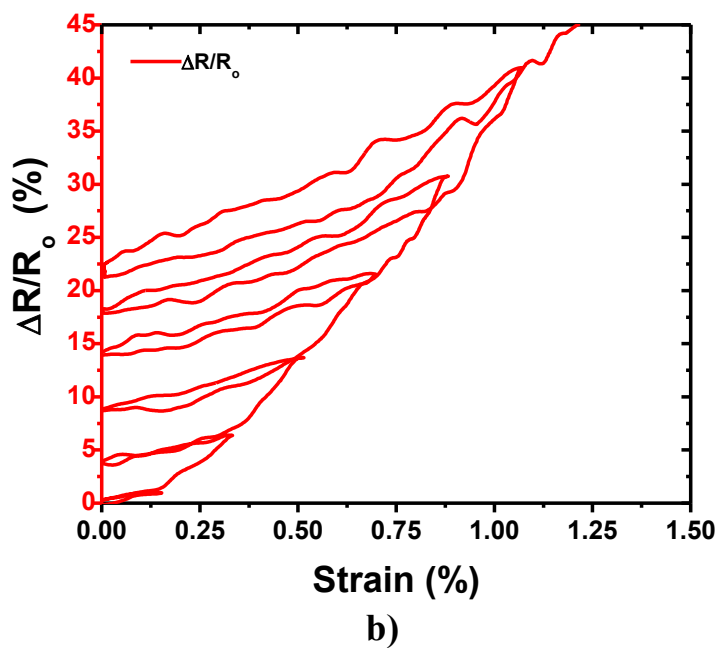
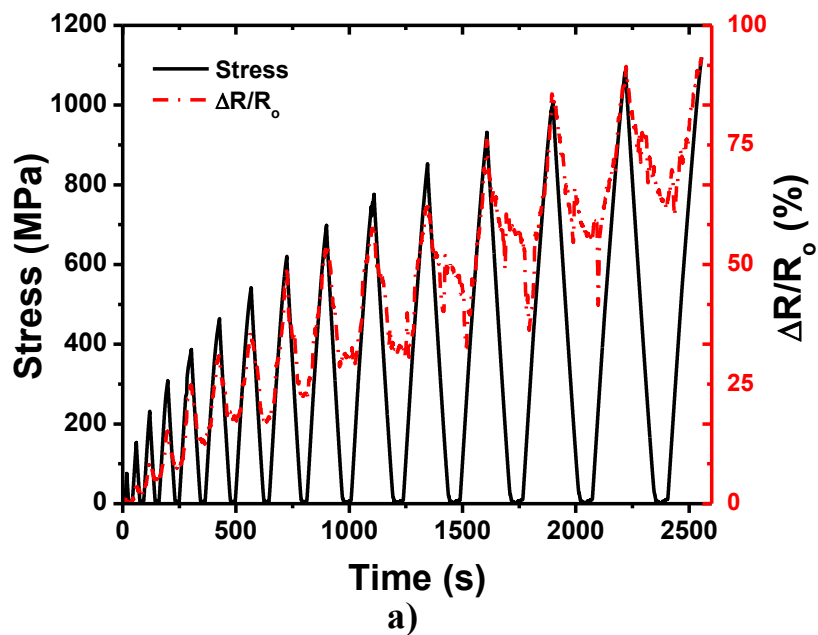


Figure 4.5: (a) Cyclic loading-displacement-resistance plots for xGnP sensor and (b) resistance-strain plot.

Limited elastic recovery and large changes in resistance between cycles for the xGnP pattern indicates the sensor is less robust than its carbon nanotube counterpart. In Figure 4.5 (b) the absence of a linear elastic region and knee produces a false reading of damage at lower loadings. Consequently, the unloaded resistance value correlates well to the resistance at the maximum strain of the prior load step, creating a sensor that provides max-strain data as opposed to information on the state of damage. The crack reopening and crack closure curves share a similar positive slope, enabling accurate extrapolations of the maximum strain value while knowing the resistance and strain at a given point in time. A sensor with this capability could be utilized in a system where knowledge of the maximum strain experienced is desired without having to support the power-intensive, always-on SHM system but in a NDE application that collects data intermittently.

4.4 Time-Invariant NDE Approaches

Developing methods to quantitatively analyze the electrical response of the patterned sensors is a required step before any practical implementation of this technology. With consideration for creating low-power and low weight systems utilizing minimal instrumentation, different means to assess damage are discussed.

This technique uses the baseline resistance measurements to collect data in between loading cycles, or service intervals, and works well within the framework of current NDE practices. Continuous sensing of time and strain information is not required. Figure 4.6 (a) and (b) qualitatively address the use of the baseline resistance in terms of load cycle number, not time.

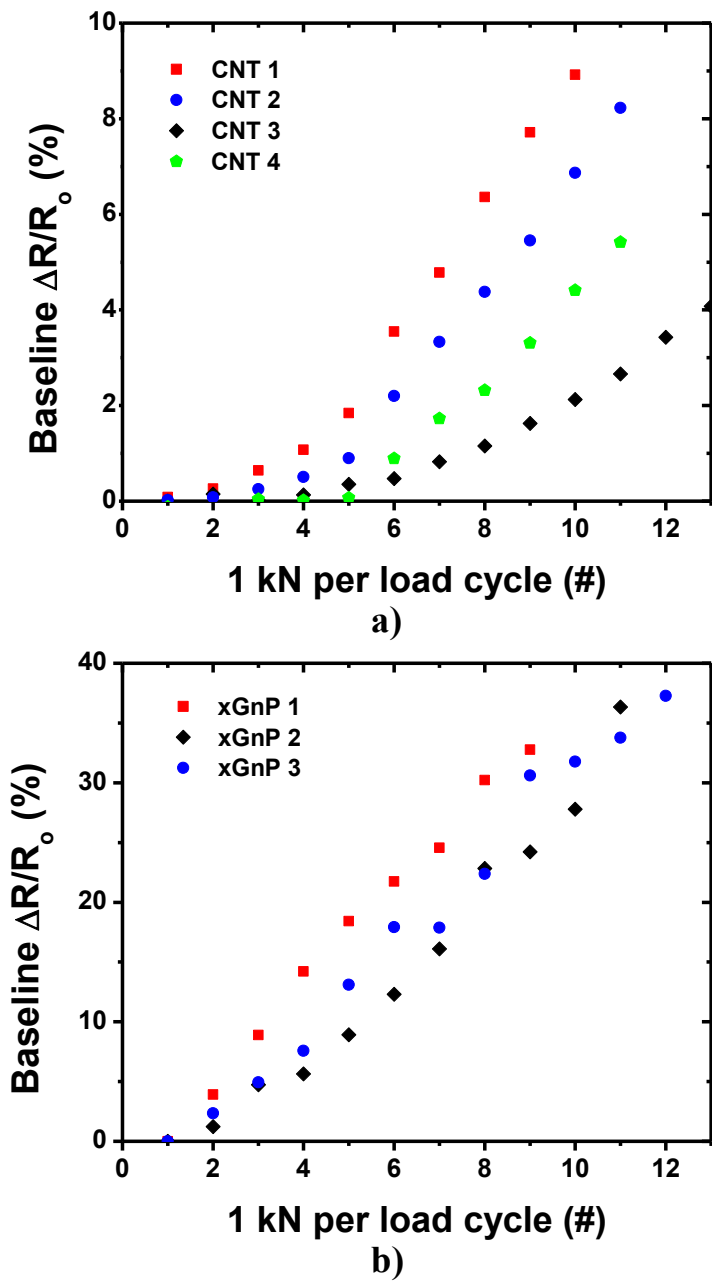


Figure 4.6: Baseline method for carbon nanotube (a) and xGnP (b) sensing networks subjected to progressive cyclic tensile loading.

By observing the baseline and load number information alone, it is possible to construct a damage progression curve. The behavior of the resistance change for the carbon nanotube data sets, Figure 4.6 (a), is analyzed with a quadratic regression, while results for the xGnP data sets, Figure 4.6 (b), utilize linear regression. Explanation of these behaviors is consistent with the monotonic tensile test; with the carbon nanotubes sensing individual fiber damage events resulting in a stepped behavior, which when sampled over an interval follows a second order polynomial. The xGnP is linear with the applied load and serves as a measure of strain. Again, the variability in each sensor's sensitivity range is apparent with the large distribution of failure change resistance for carbon nanotube sensors versus a narrow range for xGnP. Sensitivity range values for each pattern type can be measured and used for calculation of the failure probability using baseline resistance measurements.

4.5 Analysis of Damage Progression and Failure Mechanisms for SHM

Always-on SHM systems must be able to provide additional information than their NDE counterparts to justify their extra expense. Through utilizing AE data to identify fiber fracture events it is possible to elucidate the damage mechanisms at present affecting the interface sensor's response. The the ability to detect incipient damage for the carbon nanotube sensors enable a more in-depth analysis of the resistance behavior as damage accrues within the composite.

This approach evaluates the nonlinear resistance response during loading which is typically comprised of three distinct segments. A similar nonlinear phenomena for carbon nanotube-modified matrix materials in fiber reinforced composites has been previously studied by Gao and Thostenson [43]. Gao characterized the three regions as crack reopening, elastic response, and new damage.

A significant difference from this prior study stems from the nature of the composites and the sensor implementation. Gao studied cross-ply specimens for damage sensing in the matrix with continuous carbon nanotube dispersion throughout the composite, while this study explores unidirectional specimens with nanotube-based sensors concentrated at the fiber/matrix interface.

The carbon nanotube response signal in Figure 4.7 (a) offers an opportunity to detect the complex nature of the onset and accumulation of damage within composite materials. The cyclic carbon nanotube damage response is presented with AE data that marks magnitude of energy released, which can be used to understand the damage progression.

Figure 4.7 (b) assumes an ideal material, but conservative engineering practices require we make assumptions regarding the heterogenous composition of composite materials and their microstructure. Challenges exist due to the fiber strength distribution which is a consequence of natural production variations in the reinforcing fiber, random packing of the micron sized fibers throughout the composite cross section, and, finally, the dispersion quality and orientation of nanomaterials at the fiber and matrix interface, as shown in Figure 4.7 (c).

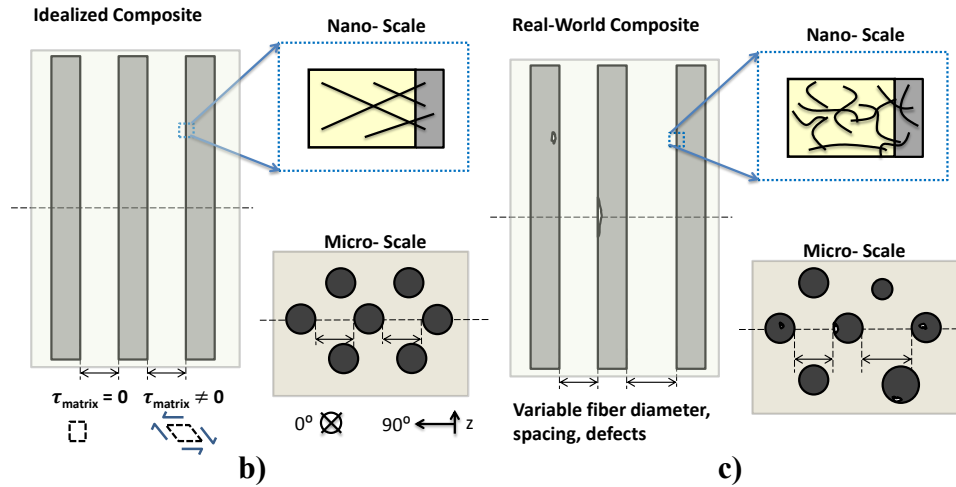
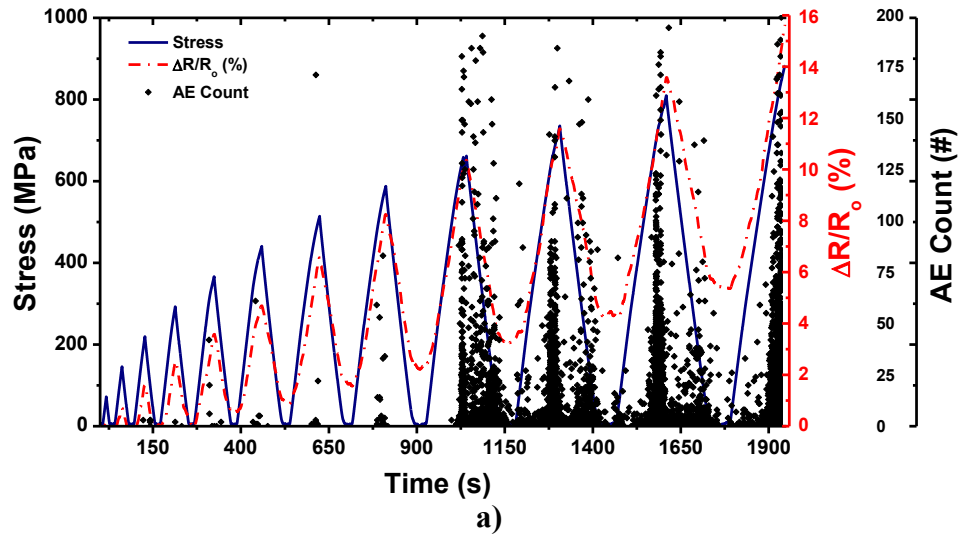


Figure 4.7: (a) Carbon nanotube cyclic response with AE emissions, and a illustrate depicting the macro-, micro-, nano-scale structure of (b) idealized and (c) real world composites.

Up to the first acoustic event during the third load, circled in Figure 4.8 (a), there is a linear resistance response during both loading and unloading, suggesting an elastic response. AE events result from the release of stress waves from a fiber fracture event. Since the failure of the weakest fibers at low loads release limited strain energy, there is little fiber/matrix interface debonding, as reflected by absence of new damage in the baseline resistance as illustrated in Figure 4.8 (b). During subsequent loading, these fractured fibers create stress concentrations and initiate matrix cracking which is observed in the resistance response. To aid in the visualization of the complex state of stress within the matrix dashed elements are used to represent the in-plane shear stress. Square elements correspond to no shear resulting in zero change in resistance. Deformed elements represent shear being transmitted through the matrix which degrades the electrically conductive network.

Local variability in fiber strengths creates non-uniform stress distributions in the matrix, shown in Figure 4.8 (c). The local break in the fiber results in load transfer to nearby intact fibers via shear which induces a piezoresistive response of the interfacial carbon nanotube network as electrical pathways are strained, γ . The nonlinear resistance behavior of the first region of the cycle after the initial AE events indicate the reopening of the fracture surfaces produced by the failure of the weakest fibers. The second regime corresponds to the specimen's elastic response and terminates once the loading has reached the maximum value of the prior load cycle, as indicated with the horizontal arrows. Beyond this load, new fracture events are recorded, indicating the initiation of the new damage resistance response region. During this time, interfacial debonding occurs near the ends of failed fibers, which is reflected in the change of the baseline resistance.

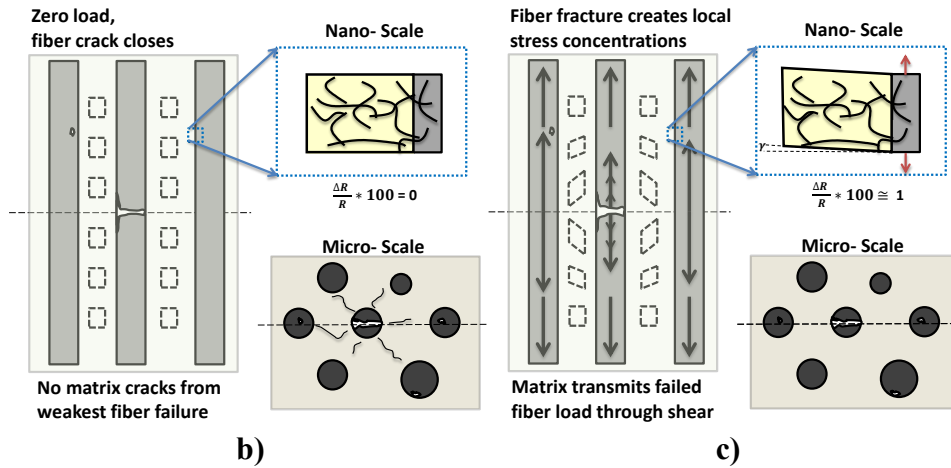
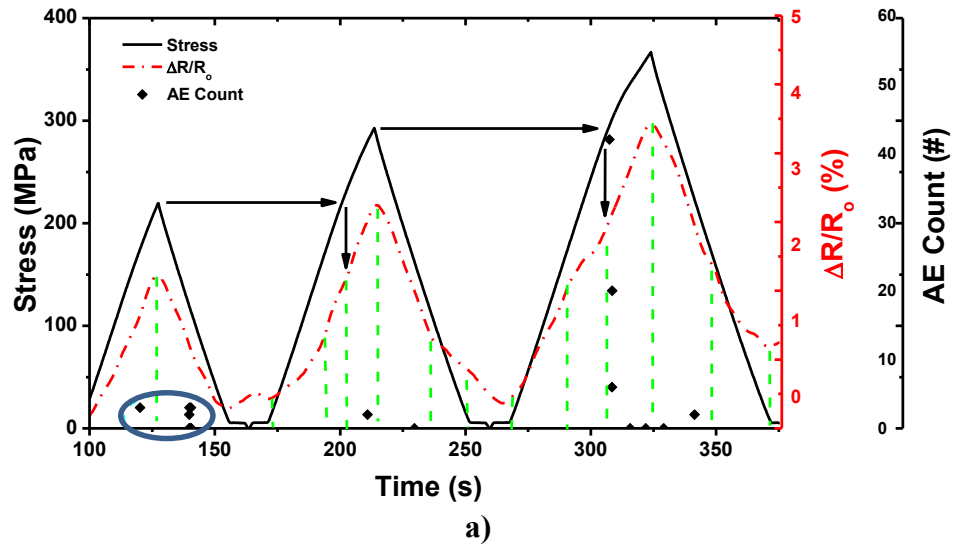
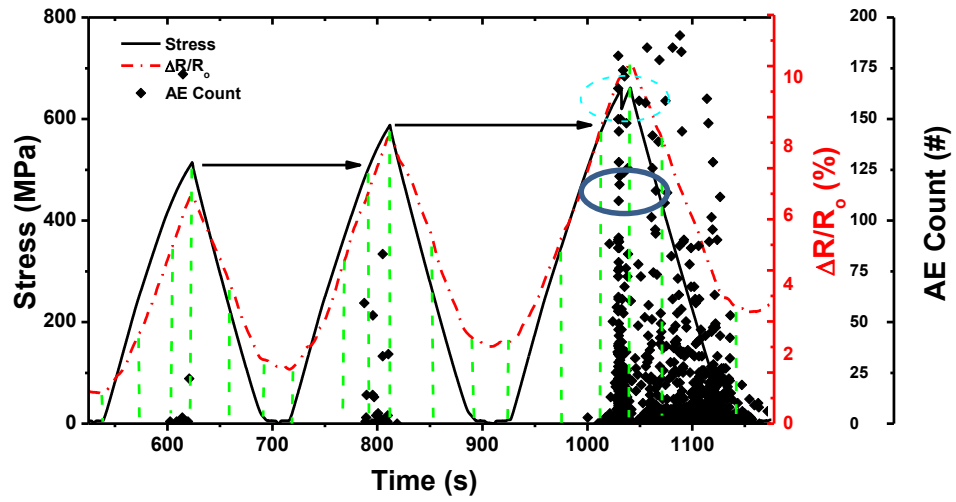


Figure 4.8: (a) Plot of the 3rd, 4th, 5th cycle, where damage first initiates, as indicated by the circled AE events. The dashed green lines indicate a change in the mechanism affecting the resistance response. The illustrations highlight the differences in the state of stress in composites with initial fiber fractures under no applied load (b) and with applied load (c).

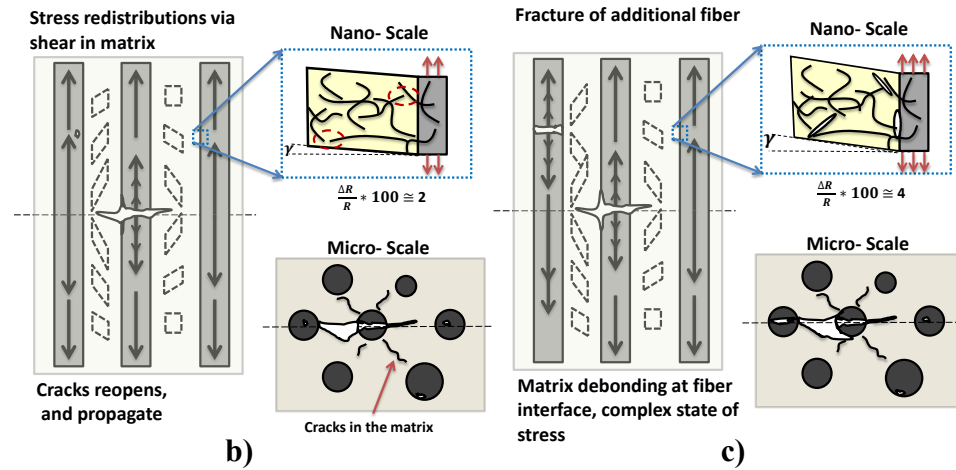
The nonlinear unloading curve's first region corresponds to the recovery of the initial elastic deformation of the composite. During elastic unloading and crack closure, the electrically conductive pathways reconnect and lower the resistance. The second part of unloading relates to the closing of preexisting cracks. Similar damage accumulation behavior continues in later cycles up to ultimate composite failure.

In Figure 4.9 (a), a new damage region in the first two cycles show an increased acoustic events. The following cycle records a significant increase in AE events. Shear lag analysis considers the interaction at the fiber ends and matrix to determine its ability to transmit shear, however a debonding at the fiber and matrix interface is also possible, enabling frictional sliding of the fiber. It is possible that the fibers have debonded from the deposited sensor media and matrix material, and begun to slide.

An optical micrograph in Figure 4.10 shows long fibers protruding from the fracture surface indicating the fibers have debonded and pulled-out of the matrix. This dissipation of strain energy would explain the abundance of acoustic events during the new damage and unloading regions, as no permanent damage in the resistance signal would be associated with the frictional sliding corresponding to the acoustic events. The circled load drop at the maximum of the 9th cycle indicates a large failure event, possibly corresponding to large-scale interfacial debonding. Figures 4.9 (b) and (c) illustrate conditions contributing to complex states of stress in the fibers and matrix and the resultant larger piezoresistive response of the interfacial sensor.



a)



b)

c)

Figure 4.9: (a) Plot of 7th, 8th, and 9th load cycle during the transition to a new damage mechanism, where (b) illustrates the state of stress prior to the shift, and (c) the complex state of stress afterwards.

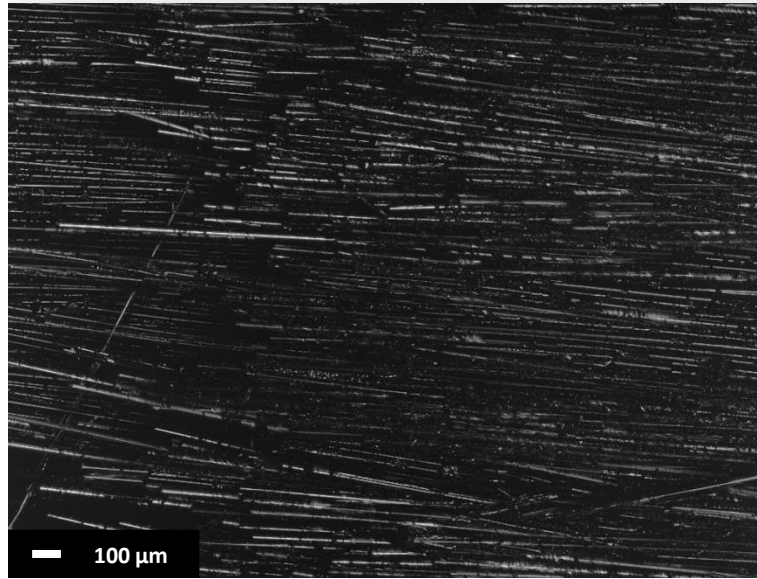


Figure 4.10: Optical micrograph of protruding fibers indicative of fiber debonding from the matrix at the carbon nanotube fracture surface within the patterned region.

4.6 Summary

Sensing capabilities for xGnP and carbon nanotube based discrete sensors have been established. The xGnP printed sensors do not penetrate the fiber bundles and rest on top of the fibers and act as integrated interlaminar strain gages. Carbon nanotube patterns penetrate the fiber bundles and are highly sensitive to damage events. First fiber fracture events can be identified in the resistance-strain response.

The sensitivity ranges for both types of specimens is determined and can be used to predict the probability of failure of a composite given its baseline resistance and measured resistance at an unloaded state. Carbon nanotube sensors display a wide sensitivity range, owing to their sensitivity in detecting micro-scale damage, making them poorly suited for this type of sensing. The xGnP sensors have a well-defined sensitivity range and have potential to work well in this type of NDE implementation.

Analysis of the carbon nanotube nonlinear resistance response during loading cycles allows for identification of the damage mechanisms. For SHM applications the regions of the nonlinear response have been identified as crack reopening, elastic response, new damage, closing of new fracture surfaces, and elastic closure of initial fracture surfaces. Sensors produced from xGnP experience signal degradation with increased levels of noise with accumulated damage, making detailed analysis impractical.

Chapter 5

CONCLUSIONS AND FUTURE WORK

5.1 Conclusions

Research on carbon nanotube and xGnP nanocomposite processing and piezoresistivity has established a foundation that can be used to better understand *in situ* damage sensing methods.

The influence of processing on xGnP nanocomposite strength and resistivity was been studied and the appropriate processing conditions for self-sensing capability have been determined. Damage onset and matrix cracking is observed beyond the transition point from the linear range of electrical response during loading. The propagation of damage is apparent in the deviation of the materials resistance response between loading cycles. The distinct nonlinear electrical response during loading and linear unloading each demonstrate a progressive change in slope that directly relates to the extent of damage in the nanocomposite. Utilization of the crack reopening and crack closure slope progression could be used in conjunction with a known input force for a dynamic testing of structural integrity. The development of methods to analyze the electrical resistance response of the xGnP conductive network warrants further research on xGnP hybrid nanocomposites. This work is the first of its kind to study processing relationship of graphene for sensing applications in thermosetting resins and serves as a basis for future research in more complex material systems.

An adapted screen printing process has been utilized for the deposition of *in situ* sensors onto glass fabric. Carbon nanotube and xGnP water-based dispersions (screen printing ink) create a piezoresistive network capable of damage and strain sensing respectively. The damage onset, progression, and damage accumulation

behavior of each specimen type is evaluated and identified. The sensitivity range enables probability of failure calculations knowing the baseline and current resistance.

An approach is proposed for nonlinear resistance response for sensing along the fiber matrix interface to enable more accurate capabilities to assess damage. Two robust methods of resistance data reduction for better quantitative analysis tools are introduced. The method of baselines tracks changes in the resistance between cycles and is well-suited for NDE applications, whereas the method of regions identifies the specific component of the nonlinear response that corresponds directly to damage events for real-time SHM systems. Additional experiments and modeling are required to fully validate these methodologies of interpreting the resistance data.

The ability to directly pattern sensors for discrete or active monitoring onto composite fibers is considerable step forward for the *in situ* damage sensing approach. xGnP has potential applications serving to measure strain, whereas the level of detail the interfacial carbon nanotube sensors offers for marco-level implementations.

5.2 Future Work

These initial research efforts have given rise to many additional questions which require further studies. Key areas of future work fall into two broad categories, processing and characterization methods and experimental studies.

5.2.1 Processing and Characterization Methods

5.2.1.1 xGnP Microscopy Study

For xGnP processing, microscopy studies should be undertaken to correlate the observed mechanical and electrical properties with the morphology of the as-processed material. Scanning electron microscopy of fracture surfaces from tensile

bars will provide information on the diameter of the graphite platelets, and their relative distribution throughout the specimen. It is believed that the graphene nanocomposites are thermodynamically instable, and the dispersed material re-agglomerates prior to cure. Such re-agglomeration may be favorable and form a ‘super cluster’ that enables the percolating electrical network within the polymer or reduces electrical conductivity.

An earlier assumption addressed the signal degradation of the xGnP sensors where ‘few layer graphene’ particulates shearing along a basal plane during loading as the likely response. An extension of the microscopy study would be to measure the average thickness of particulates vertically and horizontally embedded in the matrix. Vertically aligned flakes are constrained in the thickness direction, and likely debonded along their edge yielding an accurate measure of particle thickness produced by milling. In contrast, the horizontally aligned platelets are only bonded to each other through van der Waals interactions, increasing the likelihood of splitting during loading.

5.2.1.2 Inkjet Printing

Inkjet printing of micron-scaled hierarchal patterns is a natural extension to the millimeter-level capability of screen printing. Figure 5.1 highlights the different processes. Current printing has a resolution of multiple fiber bundles allowing for sensor architecture on the lamina scale, however inkjet printing would take patterning one step further down to the fiber bundle level allowing sensors to be designed for specific failure mechanisms.

Axial deposition on exterior plies of a fiber preform would sense fiber fracture, whereas axial depositions on the interior could potentially measure matrix cracking in

the intra-ply matrix rich regions, indicative of delamination. Off-axis loading or loading transverse to the fiber direction, could be measured with sensors printed across the fiber width.

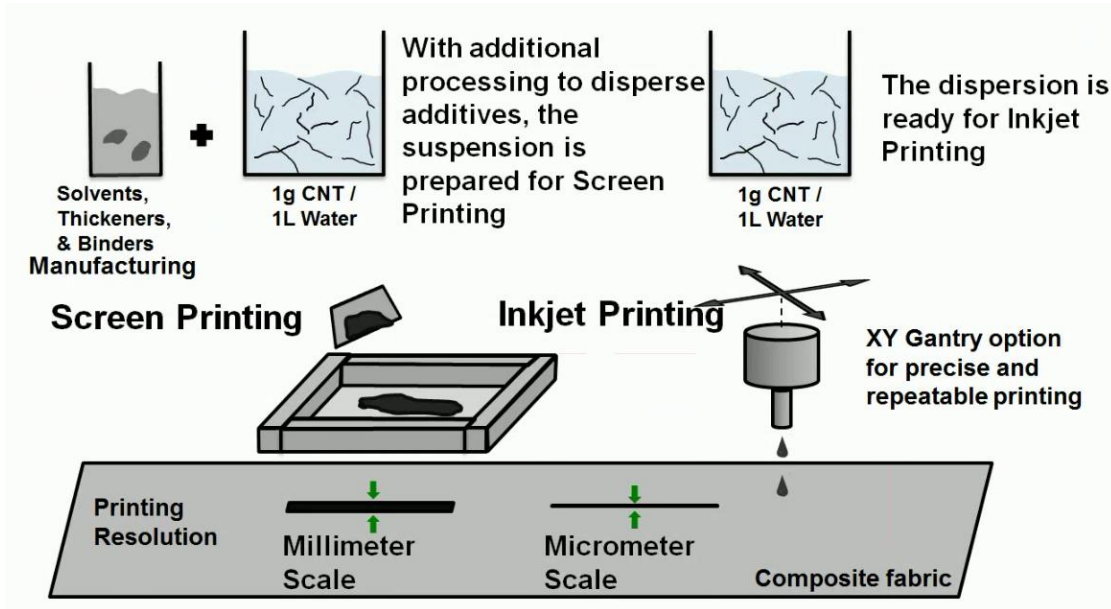


Figure 5.1: Screen printing versus inkjet printing.

5.2.1.3 Functionalized and Reformulated Inks

Improvements in ink chemistry can be realized through utilizing a method to functionalize the nanomaterials. Many such methods exist, however the ozone treatment of both carbon nanotube and xGnP for aqueous dispersions would be most industrially scalable. Current screen ink utilizes a water base and rheological modifiers that alter the pH of the final ink. The thermodynamically unstable xGnP ozone-treated solutions precipitated out of solution when the additives for screen printing were introduced. Development of a stable screen ink holds potential to expand the use of these sensors by increasing mechanical properties through better adhesion. Lowering

the surface energy of the patterning media will improve wetting which would increase the interfacial area of the sensors.

5.2.2 Experimental Studies

5.2.2.1 Sensing of Failure in Single Fiber Lamina

The application of interfacial carbon nanotube sensing could be highlighted, and more precisely studied through a more controlled test. A planar distribution of vertically aligned individual patterned fibers to make a single fiber thick composite would require precise manufacture. However, the optically clear fibers and epoxy at that thickness would allow for direct observation of the failure mechanisms through optical microscopy. A defect imposed on a central fiber along its length could be inserted to locate a camera to capture video of the failure. Exposure to polarized light will produce a isochromatic stress distribution enabling direct visualization of stress concentrations due to the materials photo elasticity. This method works well for visualizing stress distributions resulting from unknown or complicated conditions at the ends of composite fibers [48].

A dinocapture AD4113ZT has the required resolution and polarizing light built in. This would provide a definitive means to correlate the resistance response with actual damage events and mechanisms. This model is an upgraded version of the camera currently used but has the same sensor and magnification range so it can be used in conjunction with the current camera in a stereoscopic imaging setup.

5.2.2.2 Cross-Ply Composite Studies

Cross-ply composites $[0^\circ/90^\circ]_s$ with current sensor patterning approach along the transverse fibers of the 90° could sense crack onset, propagation, saturation, and

ply delamination. Sensing of these damage mechanisms has been studied earlier, but with the bulk-filling of the matrix with carbon nanotube. As with the carbon nanotube patterned sensors, it is likely that a more in-depth understanding of the failure modes would be useful. Cross-ply composites are a natural extension for the current work on nanocomposite behavior with the xGnP, and on unidirectional composites with both carbon nanotube and xGnP. Potential challenges include developing a means to gather resistance data from the interior of a specimen without introducing defects that would compromise the material performance.

REFERENCES

1. Zhou G, Sim L. Damage detection and assessment in fibre-reinforced composite structures with embedded fibre optic sensors - review. *Smart Mater Struct* 2002;11(6):925-939.
2. Leng J, Asundi A. Structural health monitoring of smart composite materials by using EFPI and FBG sensors. *Sens Actuator A-Phys* 2003;103(3):330-340.
3. An Y, Kim MK, Sohn H. Airplane hot spot monitoring using integrated impedance and guided wave measurements. *Struct Control Health Monit* 2012;19(7):592-604.
4. Overview of piezoelectric impedance-based health monitoring and path forward. *Shock Vib Dig* 2003;35(6):451.
5. Piezoelectric composites for sensor and actuator applications. *IEEE Trans Ultrason Ferroelectr Freq Control* 2005;52(5):746.
6. Eswaraiah V, Balasubramaniam K, Ramaprabhu S. Functionalized graphene reinforced thermoplastic nanocomposites as strain sensors in structural health monitoring. *J Mater Chem* 2011;21(34):12626-12628.
7. Pinto F, Ciampa F, Meo M, Polimeno U. Multifunctional SMART composite material for in situ NDT/SHM and de-icing. *Smart Mater Struct* 2012;21(10):105010.
8. Pandey G, Thostenson ET, Heider D. Electric Time Domain Reflectometry Sensors for Non-Invasive Structural Health Monitoring of Glass Fiber Composites. *Prog Electromagn Res* 2013;137:551-564.
9. Gao L, Chou T, Thostenson ET, Zhang Z, Coulaud M. In situ sensing of impact damage in epoxy/glass fiber composites using percolating carbon nanotube networks. *Carbon* 2011;49(10):3382-3385.
10. Thostenson ET, Chou T. Carbon nanotube networks: Sensing of distributed strain and damage for life prediction and self healing. *Adv Mater* 2006;18(21):2837.
11. Weibull W. A Statistical Distribution Function of Wide Applicability. *J Appl Mech -Trans ASME* 1951;18(3):293-297.

12. Rosen, B. W. (1965) Mechanics of composite strengthening, in Fibre Composite Materials. ASM: Metal Park, Ohio chapter 3
13. Zweben C, Rosen B. A Statistical Theory of Material Strength with Application to Composite Materials. J Mech Phys Solids 1970;18(3):189
14. Phoenix S, Beyerlein I. Distributions and size scalings for strength in a one-dimensional random lattice with load redistribution to nearest and next-nearest neighbors. Phys Rev E 2000;62(2):1622-1645.
15. Gojny F, Wichmann M, Fiedler B, Bauhofer W, Schulte K. Influence of nano-modification on the mechanical and electrical properties of conventional fibre-reinforced composites. Compos Pt A-Appl Sci Manuf 2005;36(11):1525-1535.
16. Schulte K, Baron C. Load and Failure Analyses of Cfrp Laminates by Means of Electrical-Resistivity Measurements. Composites Sci Technol 1989;36(1):63-76.
17. Thostenson ET, Chou T. Carbon nanotube networks: Sensing of distributed strain and damage for life prediction and self healing. Adv Mater 2006;18(21):2837-+.
18. Cook J, Evans C, Gordon J, Marsh D. Mechanism for Control of Crack Propagation in All-Brittle Systems. Proc R Soc Lond A-Math Phys Sci 1964;282(1390):508-+.
19. He M, Evans A, Curtin W. The Ultimate Tensile-Strength of Metal and Ceramic Matrix Composites. Acta Metall Mater 1993;41(3):871-878.
20. Evans A, Zok F. The Physics and Mechanics of Fiber-Reinforced Brittle-Matrix Composites. J Mater Sci 1994;29(15):3857-3896.
21. Qian H, - Greenhalgh ES, - Shaffer MSP, - Bismarck A. - Carbon nanotube-based hierarchical composites: a review. - J Mater Chem(- 23):- 4751.
22. Fan Z, Hsiao K, Advani S. Experimental investigation of dispersion during flow of multi-walled carbon nanotube/polymer suspension in fibrous porous media. Carbon 2004;42(4):871-876.
23. Lim AS, Melrose ZR, Thostenson ET, Chou T. Damage sensing of adhesively-bonded hybrid composite/steel joints using carbon nanotubes. Composites Sci Technol 2011;71(9):1183-1189.

24. Kazani I, Hertleer C, De Mey G, Schwarz A, Guxho G, Van Langenhove L. Electrical Conductive Textiles Obtained by Screen Printing. *Fibres Text East Eur* 2012;20(1):57-63.
25. Kalaitzidou K, Fukushima H, Drzal LT. Mechanical properties and morphological characterization of exfoliated graphite–polypropylene nanocomposites. *Composites Part A: Applied Science and Manufacturing* 2007;38(7):1675-1682.
26. Khan U, May P, O’Neill A, Coleman JN. Development of stiff, strong, yet tough composites by the addition of solvent exfoliated graphene to polyurethane. *Carbon* 2010;48(14):4035-4041.
27. Graphene/Polyurethane Nanocomposites for Improved Gas Barrier and Electrical Conductivity. - *Chem Mater*(- 11):- 3441.
28. Effect of Chemical Modification of Graphene on Mechanical, Electrical, and Thermal Properties of Polyimide/Graphene Nanocomposites. - *ACS Appl Mater Interfaces*(- 9):- 4623.
29. Pumera M, Ambrosi A, Bonanni A, Chng ELK, Poh HL. Graphene for electrochemical sensing and biosensing. *Trac-Trends in Analytical Chemistry* 2010;29(9):954-965.
30. Kuila T, Bose S, Khanra P, Mishra AK, Kim NH, Lee JH. Recent advances in graphene-based biosensors. *Biosens Bioelectron* 2011;26(12):4637-4648.
31. Kim KS, Zhao Y, Jang H, Lee SY, Kim JM, Kim KS, Ahn J, Kim P, Choi J, Hong BH. Large-scale pattern growth of graphene films for stretchable transparent electrodes. *Nature* 2009;457(7230):706-710.
32. Bonaccorso F, Sun Z, Hasan T, Ferrari AC. Graphene photonics and optoelectronics. *Nature Photonics* 2010;4(9):611-622.
33. Wei W, Qu X. Extraordinary Physical Properties of Functionalized Graphene. *Small* 2012;8(14):2138-2151.
34. Georgakilas V, Otyepka M, Bourlinos AB, Chandra V, Kim N, Kemp KC, Hobza P, Zboril R, Kim KS. Functionalization of Graphene: Covalent and Non-Covalent Approaches, Derivatives and Applications. *Chem Rev* 2012;112(11):6156-6214.

35. Song P, Zhang X, Sun M, Cui X, Lin Y. Synthesis of graphene nanosheets via oxalic acid-induced chemical reduction of exfoliated graphite oxide. *RSC Adv* 2012;2(3):1168-1173.
36. Dreyer DR, Park S, Bielawski CW, Ruoff RS. The chemistry of graphene oxide. *Chem Soc Rev* 2010;39(1):228-240.
37. Novoselov, K. S.; Geim, A. K.; Morozov, S. V.; Jiang, D.; Zhang, Y.; Dubonos, S. V.; Grigorieva, I. V.; Firsov, A. A. (2004). Electric Field Effect in Atomically Thin Carbon Films. *Science* 306 (5696): 666–669
38. Wiggins KM, Brantley JN, Bielawski CW. Methods for activating and characterizing mechanically responsive polymers. *Chemical Society Reviews* 42.17 (2013): 7130-7147.
39. xGnP® Graphene Nanoplatelets. http://xgsciences.com/wp-content/uploads/2012/10/10-15-13_xGnP-M_Data-Sheet.pdf
40. Andrews R, Jacques D, Minot M, Rantell T. Fabrication of Carbon Multiwall Nanotube/Polymer Composites by Shear Mixing. *Macromolecular Materials and Engineering* 2002;287(6):395-403.
41. Gilleo K. Rheology and Surface Chemistry for Screen Printing. *Screen Printing*. February 1989:128--132.
42. Godara A, Gorbatiikh L, Kalinka G, Warriier A, Rochez O, Mezzo L, Luizi F, van Vuure AW, Lomov SV, Verpoest I. Interfacial shear strength of a glass fiber/epoxy bonding in composites modified with carbon nanotubes. *Composites Sci Technol* 2010;70(9):1346-1352.
43. Thostenson ET, Chou T. Processing-structure-multi-functional property relationship in carbon nanotube/epoxy composites. *Carbon* 2006;44(14):3022-3029.
44. Thostenson ET, Gangloff JJ, Jr., Li C, Byun J. Electrical anisotropy in multiscale nanotube/fiber hybrid composites. *Appl Phys Lett* 2009;95(7):073111.
45. S. Fredrich, L. Gao, A. Lim, E. Thostenson, "Processing and Electrical Characterication of Nanocomposites for Damage Detection on Composite Joints", 2010.
46. Surface Preparation of Composites. <http://www.vishaypg.com/docs/11183/VMM-19.pdf>

47. Gao L, Thostenson ET, Zhang Z, Chou T. Coupled carbon nanotube network and acoustic emission monitoring for sensing of damage development in composites. *Carbon* 2009;47(5):1381-1388
48. Tyson WR, Davies GJ. A photoelastic study of the shear stresses associated with the transfer of stress during fibre reinforcement. *British Journal of Applied Physics* 1965;16(2):199-205.

Appendix A

DATA ACQUISITION SYSTEM

A.1 Introduction

A new data acquisition system was designed to meet the evolving needs of the research group and alleviate scheduling difficulties for the current data acquisition system. To reduce programming complexity and make the system accessible to everyone in the lab group a hardware system composed of multiple cards contained within a single enclosure was selected. Using National Instrument hardware within the LabVIEW software environment is significantly easier than writing protocols to interface with equipment through the slower GPIB connection to individual pieces of equipment, like those manufactured by Keithley Instruments.

The physical cart (shown in Figure A.1) was designed to maximize re-configurability and user ergonomics. 80/20 extruded aluminum allows for the ability to reposition shelves. The slide-out shelf holds the wireless keyboard and mouse. The height of the top surface of the cart allows for use as a standing desk, and a mounting arm for the monitor is used to allow for repositioning of the screen. The mounting arm is also used as a lab stand and is most commonly used to mount cameras to record research experiments. Transparent polycarbonate shelving allows for easy viewing of material stored on lower shelves.

Performance concerns of the cart included heat and power distribution. The expanded steel mesh was selected to allow air flow through the system to prevent over heating. A universal power supply and surge protector was added to provide clean power to the equipment and allow for mobile use of the cart without having to shut down all the equipment.

Interior dimensions of the cart were designed to allow for the addition of a second data acquisition chassis to support additional data acquisition hardware. The slide out shelf also has a spot to drop in a plastic storage tote, which are commonly used within the lab for transporting specimens. Additional cabling for the PC and data acquisition system is stored within a plastic tote located on the main shelf. Equipment literature is also stored here.



Figure A.1: Picture of data acquisition system built into a cart.

A.1.1 Hardware

A.1.1.1 Equipment list

8 Module Chassis	PXIe-1062Q
Connectivity	
PXIe-8370:	MXI-Express x4 - PCI Express card compatibility
PXI-GPIB:	GPIB interface
PXI-4300:	8 Channel Analog Input
Strain	
PXIe-4330:	8 Channel Bridge Input
Resistance	
PXI-4022:	Guard and Current Amplifier
PXI-4071:	7.5 digit Digital Multimeter
PXI-2530B:	128 Channel Reed Relay Multiplexer; 1, 2, and 4 wire configurations
Controller	
PXIe-PCIE8370:	PCI card for host PC

A.1.2 Pictorial guide for equipment use

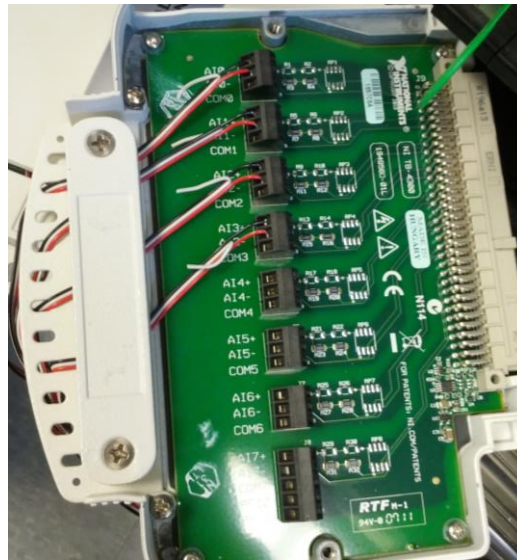


Figure A.2: The analog signal card is located in the fourth slot of the chassis, and has eight channels labeled 0 to 7 that can be interfaced. Channels zero to three are wired to the bulkhead in Figure A.5).

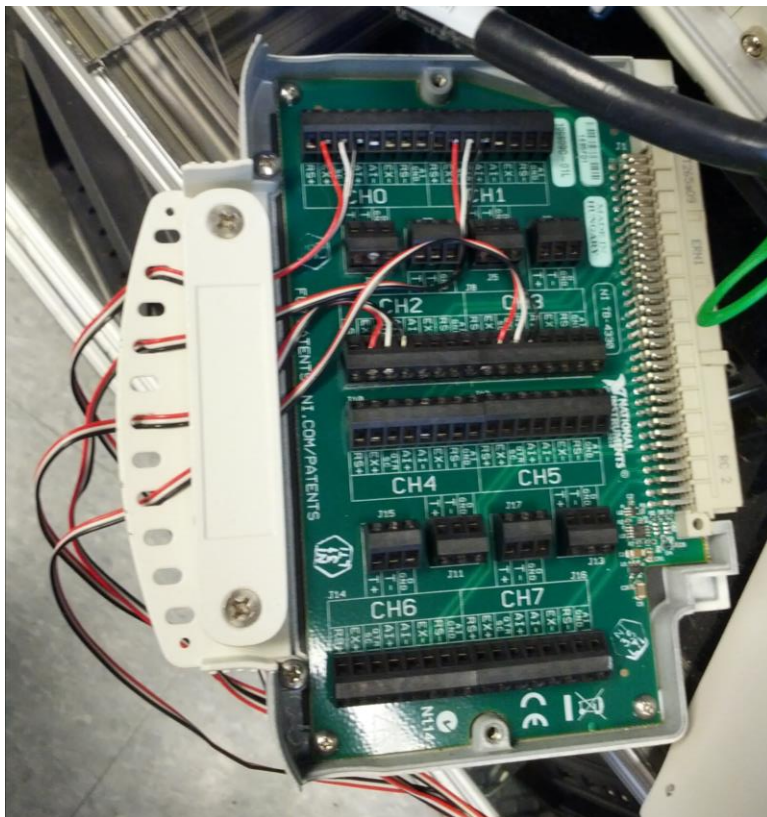


Figure A.3: The eight channel strain bridge terminal block is wired for quarter-bridge configurations, but half- and full- strain bridge configurations are possible.

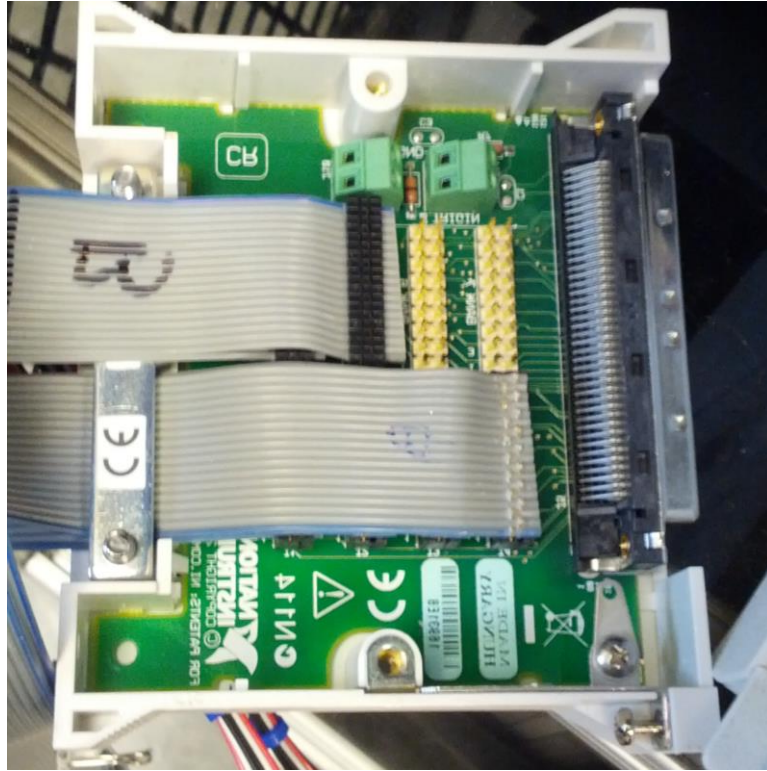


Figure A.4: The multiplexer terminal block sits in the eighth slot of the chassis and has four regions of which three have been interfaced with the ribbon cable. Two ribbon cables are required to use each of the four regions. These regions have two sets of 16 nodes, labeled 0 to 15 and 16 to 32. Additional ribbon cable and terminal blocks are stored on the cart for swapping out cable for new multiplexing applications, i.e. reconfiguring a two wire to four-wire multiplexer. Current configuration on the first two regions is for two wire multiplexing across 30 distinct regions and is instrumented in the upper half of the wiring data panel in Figure A.5



Figure A.5: The wiring panel built in the cart serves as a wire pass through or bulkhead. Additionally the reconfigurable nature of the components allows for the simple redesign for new experiments. A 30 channel, two wire multiplexer is positioned in the upper half of the panel. The lower half has four BNC pass through slots for the strain bridge (S3-#) and four analog signals (S4-#).

A.2 Troubleshooting

The four most basic programs a user can use to identify the most common problems are discussed.

A.2.1 Measurement and Automation Explorer (MAX)

If the chassis is not being recognized in MAX, it is likely the PC was turned on before the chassis. The PCI connection in the computer requires the signal be ‘hot’ before the computer turns on so that the BIOS recognizes the card. Issues with individual cards in the chassis can be diagnosed with self-tests and soft front panels.

A.2.2 DMM Soft Front Panel

Issues pertaining to the digital multimeter wiring and commands within .vi code can be time consuming and difficult to trouble shoot. Instead using the built in soft front panel to directly use a function or setting on the multimeter to test against a control specimen can be used to determine if the hardware is functioning properly and vindicate any concern of programming errors in the code or vice versa.

A.2.3 NI Switch Soft Front Panel

Like the DMM soft panel, the switch soft panel can be used to directly connect the com line to a given node for troubleshooting purposes. There is a second set of loaded electrical lead wires attached to the 30x 2-wire multiplexer and are coiled next to the chassis and run to the com line in the multiplexer terminal block. Make sure these are attached to the DMM, and not the other set of wires used during normal operation.

A.2.4 NI LabVIEW SignalExpress

If a user is experiencing difficulty in creating an executable .vi file in LabVIEW using the object based programming, using signal express will allow the user to create programs in a more intuitive fashion. Signal express programs can later be converted to .vi files and aid in learning how the software and hardware work together.

A.3 Software

A.3.1 Programs and Usage

Multiple variants of the core .vi file for data acquisition have been developed for specific testing needs. The most basic program supports load, two strain channels, and resistance input for use in most quasi static monotonic and progressive cyclic tensile tests. A more advanced program multiplexes resistance across six different nodes, and is discussed in Figure A. 6) and Figure A.7)

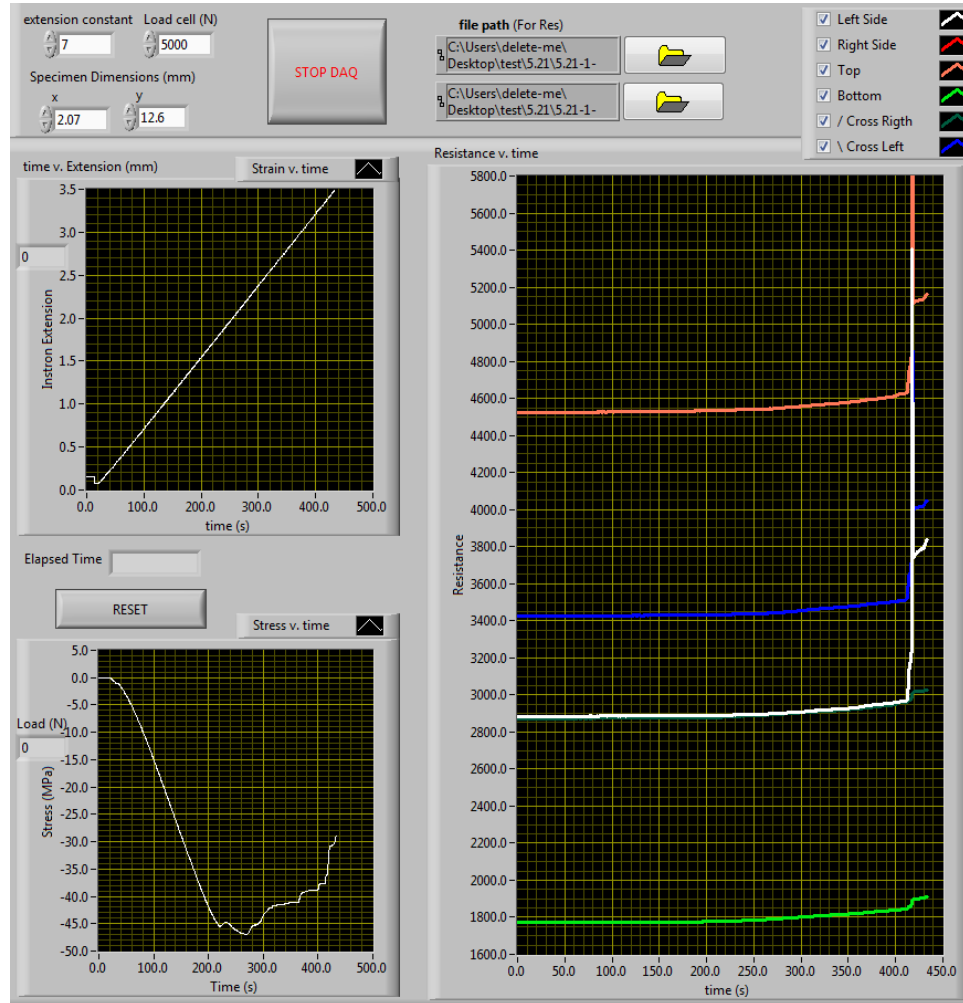


Figure A.6: Front panel of data acquisition system configured to monitor six different resistance signals. Constants from instron are entered first for crosshead extension and for the load cell. Extension and load indicators are positioned along the Y axis of the stacked plots for direct comparison to load frame values. Specimen dimensions are inputted to calculate stress. Data in gathered into two files that the user can specify the location of, one for resistance and the second for stress and strain. This version configuration is designed to multiplex resistance s measurements across six nodes, and display the response in the right hand side plot.

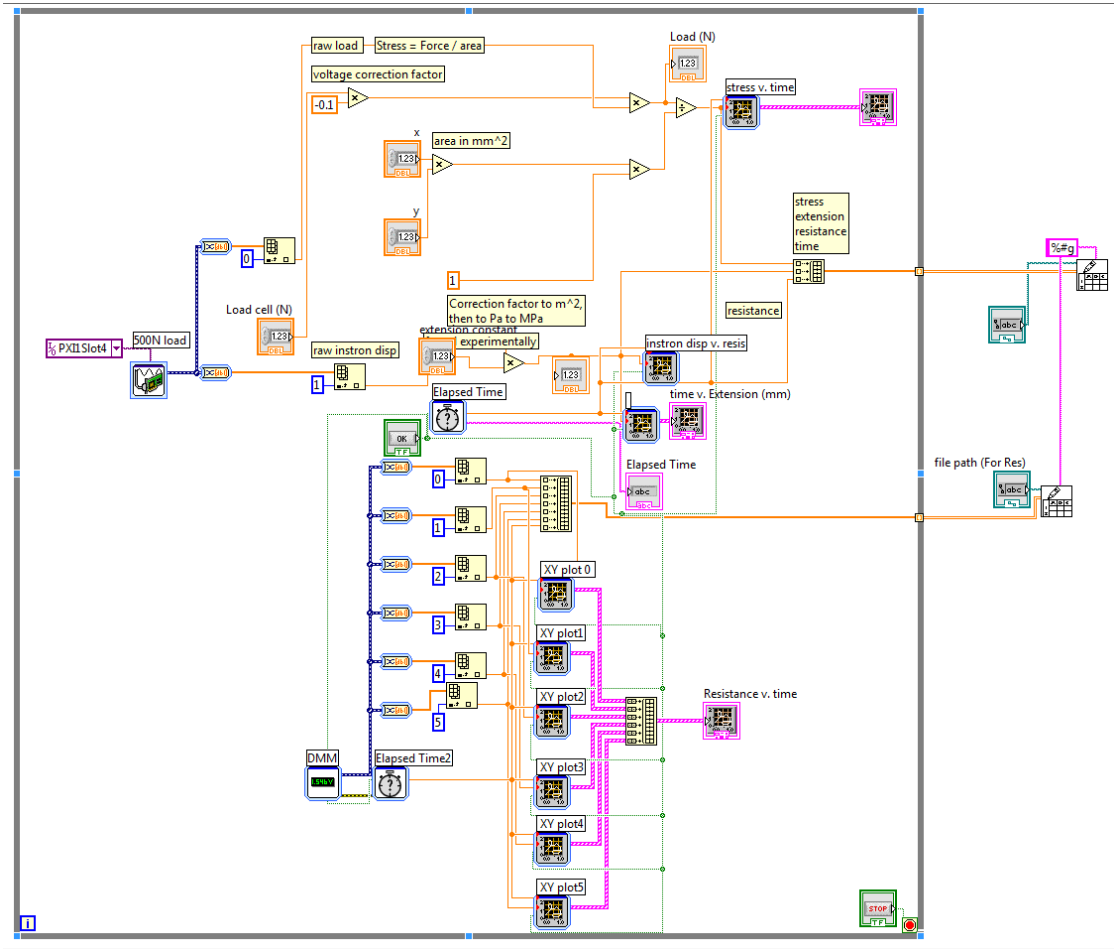


Figure A.7: Object based coding used to construct the .vi file. Users should use [control] and [h] to learn the purpose of any coding element that is not understood. The load icon controls the functions of strain and analog signals in cards three and four. The DMM icon controls the multi-meter function and switching capabilities of cards seven and eight.

Appendix B

CITATION NOTE

B.1 Figure and Table Originality

All figures and tables presented within this document are the author's own work.